Austin, J. A., Jr., Schlager, W., et al., 1988
Proceedings of the Ocean Drilling Program, Scientific Results, Vol. 101

23. PALEOMAGNETISM OF OCEAN DRILLING PROGRAM LEG 101 SEDIMENTS: MAGNETOSTRATIGRAPHY, MAGNETIC DIAGENESIS, AND PALEOLATITUDES[1]

William W. Sager[2]

ABSTRACT

Paleomagnetic measurements were made on 913 samples from 11 holes (626B, 626C, 627B, 628A, 630A, 631A, 632A, 632B, 633A, 634A, and 635B) drilled in and around the Bahamas carbonate bank during Ocean Drilling Program Leg 101. These samples displayed a wide range of magnetic intensities (from about 1.0 A/m to 1.6×10^{-6} A/m) and magnetic behavior. Most samples were weakly magnetized and had low mean destructive fields; however, sediments from sections of several holes were strongly magnetic with stable magnetizations. Magnetic-polarity interpretations were made on a Campanian unit from Hole 627B, a mid-Oligocene unit from Hole 628A, and a Plio-Pleistocene section from Hole 633A. Sediments in the upper parts of Holes 627B, 632A, and 633A have high magnetic intensities that decay 2 to 3 orders of magnitude over depths of 5 to 18 mbsf. The pattern of decline of the magnetism and the change in mean destructive fields and geochemical conditions in these holes are consistent with diagenetic dissolution of the magnetic minerals in a suboxic or anoxic-sulfidic environment. Paleolatitudes were calculated from samples from 16 time units in 7 holes and compared to the apparent polar wander path of the North American plate.

INTRODUCTION

The scientific objectives of Ocean Drilling Program (ODP) Leg 101 were to investigate the evolution of the modern Bahamian carbonate platform and the depositional history of its sediments. Nineteen holes were drilled at 11 sites (Sites 626–636) in 4 regions of the northern Bahamas (Fig. 1). Site 626 is located beneath the axis of the Gulf Stream, in the Straits of Florida between Miami and Andros Island. Sites 627–630 constitute a transect of holes on the northern slope of Little Bahama Bank. Another transect, consisting of Sites 631–633, was drilled in southern Exuma Sound. Sites 634–636 are a cluster of holes approximately coincident with Deep Sea Drilling Project (DSDP) Site 98 in Northeast Providence Channel.

Although it was expected that the carbonate sediments of the Bahamas might be only weakly magnetic and thus difficult to paleomagnetically measure and analyze, the promise of exceptional biostratigraphic and stable isotope age constraints on these sediments provided further impetus for this study. Moreover, much of the coring was done using the advanced hydraulic piston corer (APC); numerous recent paleomagnetic studies have shown that sediments recovered with a similar system (HPC) used during DSDP drilling yielded excellent paleomagnetic results (e.g., Kent and Spariosu, 1982a, 1982b; Tauxe et al., 1984; Chave, 1984; Weinreich and Theyer, 1985). The objectives of this study were twofold. One goal was to determine the magnetic stratigraphy of several holes in order to provide age constraints for sedimentary studies as well as new information about correlation of biostratigraphic, stable isotope, and magnetic polarity time scales. Important magnetostratigraphic studies have been done on sediments of Cretaceous age from nearby DSDP Site 534 on the Blake Plateau (Ogg, 1985; Ogg and Lowrie, 1986). The other objective was to calculate paleolatitudes of various ages to be used for studies of tectonics and the long-term behavior of the geomagnetic field.

Nine hundred thirteen samples were obtained for paleomagnetic study from Leg 101 cores. Holes 627B, 628A, 631A, 632A, and 633A were the most heavily sampled, but specimens from Holes 626B, 626C, 630A, 632B, 634A, and 635B were also examined. These samples comprise several different lithologies and display a relatively wide range of magnetic behavior. Although the magnetostratigraphic studies were modestly successful and several important paleolatitudes were determined, perhaps the most interesting finding was the strongly magnetic sediments of Exuma Sound, which seem to display a diagenetic alteration of the magnetic minerals over a range of tens of meters of depth.

METHODS

Samples oriented with respect to the upcore direction were taken at various depth intervals within the cores. Nominally, the spacing was 1 sample per 1.5-m core section, but samples were taken as frequently as 2 to 3 per 1.5-m section in the upper 40 m of Holes 627B, 631A, 632A, and 633A to provide more detail of the changes in magnetic character resulting from diagenesis of Exuma Sound sediments.

The sampling technique varied with the stiffness of the sediments. In cores consisting of soft oozes, 7-cm^3 plastic boxes were pushed into the split face of the core, and the resulting sample was removed with a stain-

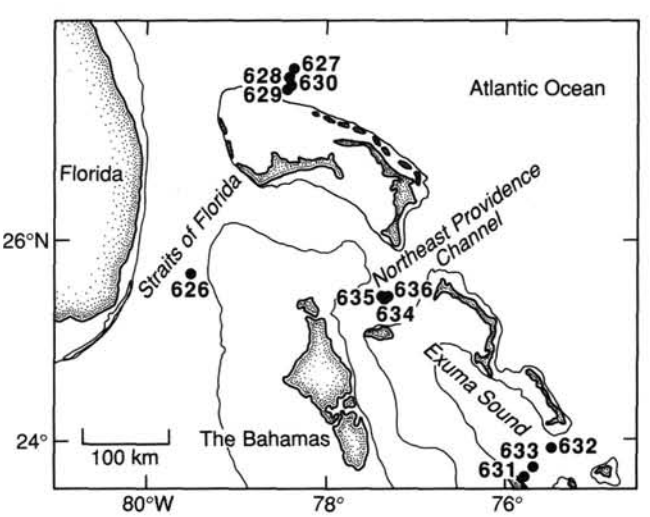

Figure 1. Locations of holes drilled during Leg 101 (from Austin, Schlager, et al., 1986).

[1] Austin, J. A., Schlager, W., et al., 1988. *Proc. ODP, Sci. Results*, 101: College Station, TX (Ocean Drilling Program).

[2] Departments of Oceanography and Geophysics, Texas A&M University, College Station, TX 77843.

less steel spatula. In stiffer sediments, samples were cut from the core with a sharpened, thin-walled 2 × 2-cm stainless steel tube. These samples were trimmed and extruded into 7-cm^3 plastic boxes. This technique was used because it tended to alleviate disturbance of the sediment that sometimes accompanies pushing a sample box into stiff core material (Karlin, 1987). A similar sampling device was successfully used on DSDP Leg 86 (Heath et al., 1985). In cores with indurated sediments, 12.4-cm^3 cylindrical minicores were drilled perpendicular to the core split face with a water-lubricated drill bit and scored with a vertical orientation mark. Only 19% of the samples were obtained by this method.

Many of the paleomagnetic samples from Leg 101 cores were weakly magnetic, and since only a spinner magnetometer was available on board the *JOIDES Resolution*, the measurements reported here were made in a shore-based laboratory. All measurements were made with a two-axis SCT cryogenic magnetometer in a mu-metal shielded room in the Department of Geological Sciences, University of Texas at Austin. The sensitivity of this instrument varied slightly with the amount of helium in its dewar and the level of electronic noise, but it was usually capable of measuring magnetization directions within 10° for samples as weak as 4.0×10^{-6} A/m. All samples were stored in the shielded room from the time they were initially measured until all measurements were completed in order to minimize spurious viscous magnetizations they might acquire from their surroundings.

Standard alternating field (AF) and thermal demagnetization techniques were used to isolate primary remanence components. These methods were applied in three levels. First, about 20% of the samples were completely demagnetized as pilot samples in steps of 5–10 milliTeslas (mT) or 50°C. These results were used to determine the best procedure for demagnetizing other stratigraphically nearby samples. For most samples AF demagnetization proved to be the preferred technique. Second, about 56% of the remaining samples were AF demagnetized at 5–10-mT steps until the measured magnetization was less than half of the natural remanent magnetization (NRM). This procedure allowed mean destructive field (MDF) values to be calculated for these samples as well as for the pilot samples. Calculation of MDF was impossible for some of the weaker samples because their demagnetized intensities were near or below the sensitivity threshold of the magnetometer. Third, the remaining samples were demagnetized in a single step selected by examining the demagnetization behavior of samples from the same core or sedimentary unit.

Because of the weak magnetization of many samples, special steps were taken to increase the accuracy and precision of the measurements. The demagnetized paleomagnetic directions listed in the Appendix are averages of six or more individual measurements. As well as decreasing the scatter from instrument noise by a factor of 2.4, this also allowed a circular standard deviation (CSD) to be calculated, using Fisher's (1953) statistics as an indicator of the reliability of each mean direction. High CSD values, in excess of 20°–30°, were interpreted to indicate unreliable inclination and declination measurements. Additionally, the plastic sample holder was routinely AF demagnetized and its magnetic moment was subtracted from the measurements of the weaker (NRM less than 5 $\times 10^{-4}$ A/m) samples.

MAGNETIC PROPERTIES

Magnetic measurements made in this study are listed in the Appendix. Paleomagnetic samples from Leg 101 can be grouped into five lithologic-magnetic categories: weakly magnetized carbonate ooze, strongly magnetized carbonate ooze, chalk, chalky limestone, and glauconitic carbonate sand.

Carbonate Ooze

Most of the samples collected for this study consist of weakly magnetic carbonate ooze. Sedimentologically, these included not only ooze but also unlithified packstone, grainstone, and partly indurated chalk. However, most samples were taken from the finer grained sediment types. These sediments in Leg 101 cores typically contain 75%–97% calcium carbonate, and some contain abundant pyrite (Austin, Schlager, et al., 1986). The carbonate-ooze samples had both strongest and weakest NRM intensities. Their NRMs were generally low, ranging from slightly greater than 10^{-6} to 10^{-4} A/m. The most weakly magnetic sample was 101-631A-4H-4, 48 cm, which had an NRM intensity of only 1.6×10^{-6} A/m. However, a small number of the carbonate-ooze samples, from Cores 101-627B-1H and 101-632A-1H to 2H and 101-633A-1H to 2H, displayed strong NRMs in the range of 10^{-4} to 10^{-2} A/m. The largest NRM intensity, 1.0 A/m, was recorded from Sample 101-632A-4H-1, 45 cm.

Under AF demagnetization, most ooze samples showed stable magnetizations with little overprint (Fig. 2). Mean destructive field values for samples of this type covered a wide range, from less than 5 mT to nearly 90 mT; however, most of the MDF values were between 5 and 50 mT. Additionally, MDF values sometimes displayed little serial correlation, as there were in some instances large differences in the MDFs of samples separated by only a few tens of centimeters.

A marked dichotomy was noted in MDF values of oozes from different holes, as shown in Figure 3. Nearly 48% of the carbonate-ooze samples from Holes 626C, 627B, 628A, 630A, and 631A had MDFs of less than 10 mT. Such low MDF values suggest that many of these samples had magnetizations that are of low stability (Fig. 2). As expected, magnetic measurements from these samples often displayed considerable scatter and were thus difficult to utilize for magnetostratigraphic or paleolatitude studies. The ooze samples from Holes 632A and 633A, however, yielded higher MDF values. About 80% of these samples had MDFs in excess of 10 mT (Fig. 3). Paleomagnetic measurements from these samples showed much less scatter than those from ooze samples in the other holes.

Although many of the carbonate-ooze samples showed a relatively stable, monotonic decay when AF demagnetized, almost all such samples treated to thermal demagnetization behaved erratically (Fig. 4). Wildly different directions and intensities of magnetization were encountered during successive heating. Furthermore, the most unstable behavior was observed at higher temperatures. After heating, the magnetizations became extremely viscous, even acquiring spurious components inside the shielded room. This behavior appears to commence in most ooze samples at temperatures of less than 150°C (the lowest setting of the oven used for this study) because orthogonal vector plots of these samples rarely displayed any systematic behavior at any of the measured temperature steps. Although a thorough investigation of this phenomenon was not undertaken, its pattern suggests that the heating may bring about a chemical change, perhaps by dewatering, that nucleates fine, superparamagnetic grains accounting for the viscous magnetism.

Because of unstable behavior upon heating, all the carbonate-ooze samples, except the thermal pilots, were studied with AF demagnetization. This procedure made it impossible to determine Curie temperatures of the magnetic minerals in most samples. The only carbonate-ooze samples that did not become unstable during thermal demagnetization were those from the strongly magnetic sediments at the top of Holes 632A and 633A. These samples apparently have Curie temperatures near that of magnetite, as will be discussed. The identities of the magnetic minerals in the other ooze samples cannot be determined with certainty from the results of this study. However, the low coercivities of these samples are consistent with the properties of magnetite.

Chalk

Although many partly indurated carbonate samples that could be categorized as chalks were recovered on Leg 101, those in Hole 627B, Cores 101-627B-27X to -34X (248.7–324.7 mbsf), and Hole 634A, Cores 101-634A-2R to -4R (144.0–172.4 mbsf), differed in two respects. They contained material that was harder than most of the other chalks recovered on Leg 101, and they were also more magnetic. These sediments generally gave good paleomagnetic results and were used for both magnetostratigraphic (Hole 627B) and paleolatitude studies.

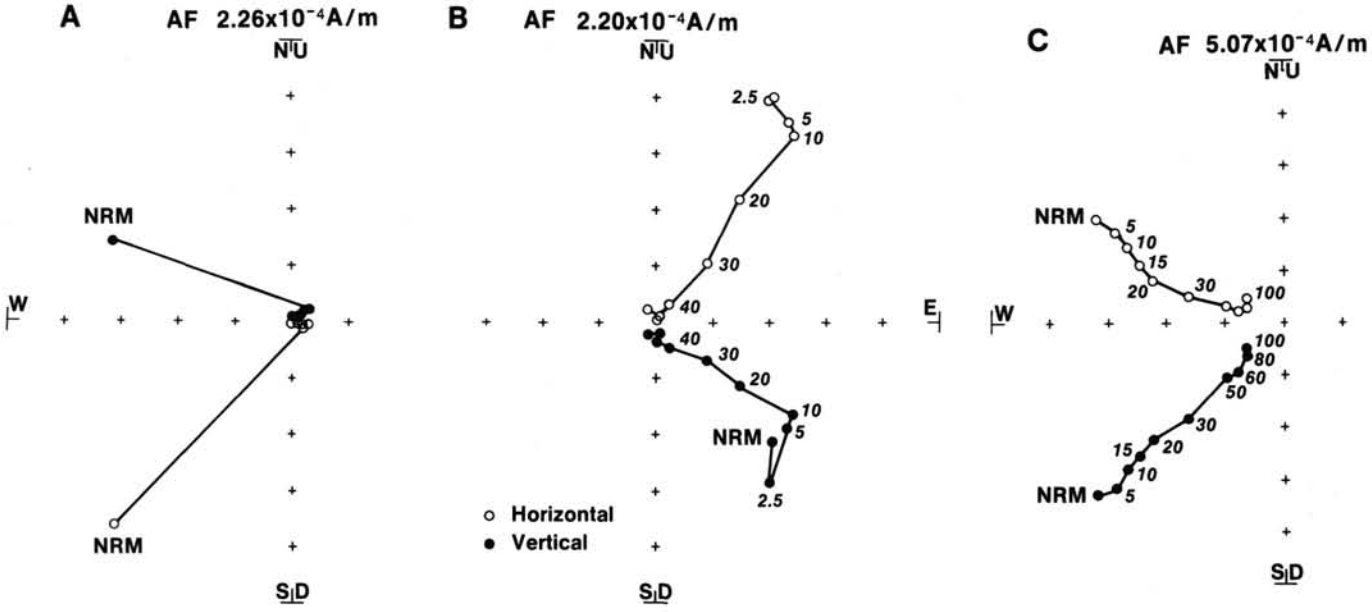

Figure 2. Orthogonal vector plots of AF demagnetization curves of typical carbonate-ooze samples. Filled circles represent projection of the magnetic vector on the east-west vertical plane; open circles show projection of the vector on the horizontal plane. Three behavior types are shown: *A*, low MDF, Sample 101-626C-16H-2, 22 cm; *B*, moderate MDF with low coercivity overprint, Sample 101-627B-14H-5, 13 cm; *C*, moderate MDF with little overprint, Sample 101-628A-9H-3, 90 cm.

In the Campanian chalk sediments of Hole 627B, most of the NRM intensities were found to be between 10^{-4} and 10^{-3} A/m. These intensities were highest in the upper part of this section, clustering around 10^{-3} A/m from about 249 to 290 mbsf. The NRM values decreased toward the bottom of the section, averaging about 10^{-4} A/m from approximately 290 to 323 mbsf (Fig. 5). For comparison, the lower Eocene chalk samples obtained from Hole 634A had NRM intensities of 10^{-5} to 10^{-3} A/m.

The chalk samples from both Holes 627B and 634A seemed to respond better to thermal than to AF demagnetization. Although AF treatment produced good results in some cases (Fig. 6), in others no stable magnetization was isolated. Furthermore, sometimes a significant portion of the magnetism remained after demagnetization to 100 mT (Fig. 6). The AF pilot samples from these holes gave MDFs that were moderate, ranging from 16 to 59 mT, with an average of 32 mT. Unlike the carbonate ooze samples, which displayed unstable magnetic behavior upon heating, the chalk could be heated to 600°C with no signs of unstable behavior (Fig. 6). Most of these samples were completely demagnetized by 600°C, and a few showed significant drops in intensity between 550° and 600°C (Fig. 7), implying a Curie temperature consistent with that of magnetite as the primary carrier of magnetic remanence.

Chalky Limestone

Dark green chalky limestone and marly chalk were sampled in Hole 627B, Cores 101-627B-37X to -47X. Somewhat similar gray limestone was sampled in Hole 635B, Cores 101-635B-8R to -14R. Both limestone units have a significantly greater organic and terrigenous material content than do other Leg 101 sediments. Additionally, both units are Cretaceous in age, specifically early to mid-Cenomanian in Hole 627B and late Albian to early Cenomanian in Hole 635B (Austin, Schlager, et al., 1986).

The NRM intensities of these limestones cluster around 10^{-4} A/m, which are stronger than most of the Leg 101 paleomagnetic samples but one or two orders of magnitude less than the strongly magnetic ooze from Exuma Sound and the Campanian chalk from Hole 627B. During demagnetization, the chalky limestone samples from both holes behaved in a manner intermediate between that of the indurated-chalk and the carbonate-ooze samples discussed previously. Generally, they displayed univectorial decay after a small overprint was removed by AF demagnetization of 20 to 30 mT (Fig. 8). Upon thermal demagnetization, however, these samples showed univectorial decay only at temperatures up to about 350° to 450°C, above which their magnetizations became unstable (Fig. 8). Despite the possible instability upon heating, most of these samples were thermally demagnetized, usually in the 200° to 300°C range, because of concern that hematite, a magnetic mineral with high coercivity, might be present in these sediments. Hematite was found in similar Mesozoic sediments in DSDP Hole 534B (Ogg, 1983), a few hundred kilometers north of the Bahamas.

Glauconitic Sand

Hole 626C sampled winnowed calcareous sand of Neogene age in the upper 112 mbsf. This sand is magnetically distinct because it contains 1% to 5% glauconite (Austin, Schlager, et al., 1986). Consequently, the sediment displayed relatively strong NRM intensities, on the order of 10^{-1} A/m. Although these samples usually behaved relatively well during AF demagnetization, some of the sand appeared to have been resuspended and redeposited by the drilling process. Consequently, the measured paleomagnetic directions were highly scattered (Appendix) and of little use for either magnetostratigraphic or paleolatitude studies.

MAGNETOSTRATIGRAPHY

Despite the large amount of material recovered using the advanced hydraulic piston corer, useful magnetostratigraphic interpretations of most of the Leg 101 cores were difficult to make because of the generally low MDFs of many of the carbonate-ooze samples and the common occurrence of thick or plentiful turbidites, slumps, and sections of poor recovery. Nevertheless, units from three holes yielded interesting magnetostratigraphic results.

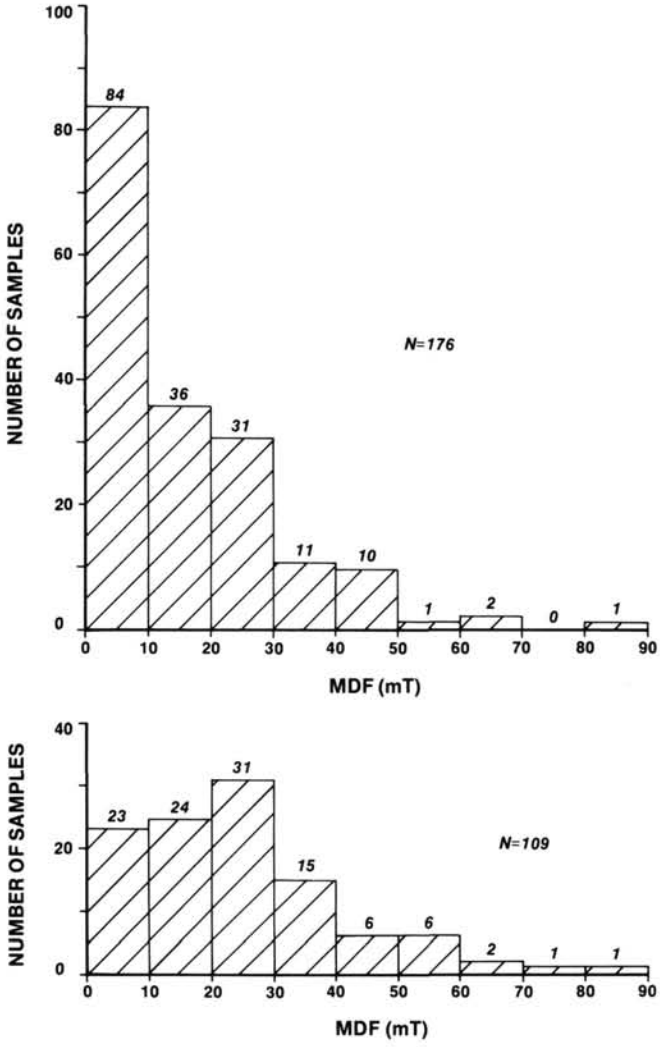

Figure 3. Histogram of mean destructive field (MDF) values for carbonate-ooze samples. Top: Holes 626C, 627B, 628A, 630A, and 631A. Bottom: Holes 632A and 633A.

Hole 627B, Cretaceous Sections

In Hole 627B, two long sections of Cretaceous sediment were recovered. One is the Campanian chalk unit in Cores 101-627B-27X to -34X (249–325 mbsf), and the other is the green Cenomanian unit in Cores 101-627B-37X to -49X (344–468 mbsf). Both were magnetized strongly enough and behaved well enough during demagnetization to indicate that they might be useful for finding reversals near the boundaries of or within the Cretaceous quiet period.

A reversal was found in the Campanian chalk unit from Hole 627B. As shown in Figure 5, samples between 250 and 259 mbsf and those below 265 mbsf within this unit display positive inclinations, implying normal polarity. At 259 to 265 mbsf, the samples yielded negative inclinations, indicating reversed polarity. One positively inclined sample, 101-627B-28X-2, 113 cm, was found within the reversal at a depth of 260.8 mbsf. It may imply a short period of normal polarity within the reversal, or it may be a single spurious result. Two other samples, at 249.1 and 306.3 mbsf, exhibit reversed polarity within normal polarity sections of the unit. In each instance the sample was obtained from the top of a core. This coincidence suggests that they have been disturbed by the drilling process; hence they probably do not record geomagnetic-field reversals.

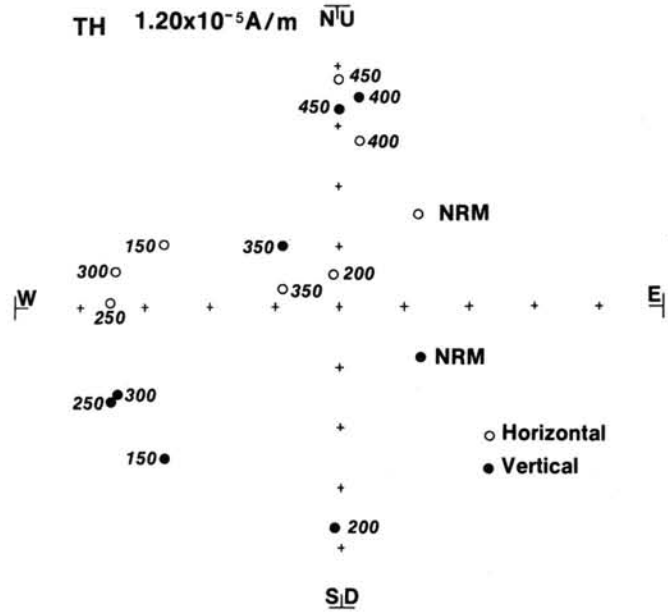

Figure 4. Orthogonal vector plot of thermal demagnetization of a typical carbonate ooze (Sample 101-628A-10H-2, 90 cm), illustrating unstable behavior. Conventions as in Figure 2.

Planktonic foraminifers and calcareous nannofossils found in these sediments indicate that the uppermost part of this chalk unit is latest Campanian in age but that the lower part extends into the middle Campanian Stage (Austin, Schlager, et al., 1986). During the early Maestrichtian and Campanian stages there were only a few magnetic-field reversals, Chrons 31r, 32r, and 33r (using the terminology of Harland et al., 1982). Chron 33r probably occurred in the early Campanian and lasted for about 4 m.y. (Kent and Gradstein, 1985), whereas the reversal found in the chalk unit appears to be short and biostratigraphically confined to the latest Campanian. Chron 31r was also relatively long, lasting for about 2 m.y. during the middle Maestrichtian. Chron 31r is probably not the reversal detected in the chalk unit because of its length. Furthermore, if the observed reversal were Chron 31r, then there would be no reversals below corresponding to Chron 32r. Thus the reversal at 259 to 265 mbsf is probably Chron 32r. The normal polarity material above and below it is thus interpreted to correspond to normal polarity Chrons 32 and 33 (Fig. 5). Additionally, the normal polarity sample within Chron 32r may record the normal polarity interval that occurred within this reversed epoch, Subchron 32r-1 (Harland et al., 1982). These results agree relatively well with published correlations of the magnetostratigraphic and biostratigraphic time scales (Berggren et al., 1985; Kent and Gradstein, 1985).

No reliable reversals were found within the green chalky limestone unit in Hole 627B, Cores 101-627B-37X to -49X. All of these sediments were apparently laid down during the Cretaceous quiet period. A few samples yielded negative inclinations (Appendix), but no two such samples occurred together, suggesting that these apparent reversals are spurious. They probably occurred from the misorientation of some samples and unstable magnetic behavior in others caused by thermal demagnetization. Calcareous nannofossils and planktonic foraminifers indicate that the sediments are early to middle Cenomanian in age and were deposited over a span of about 3–5 m.y. (Austin, Schlager, et al., 1986).

Hole 628A, Oligocene Section

The impetus for magnetostratigraphic study of cores from Hole 628A was the recovery of a long, biostratigraphically well-

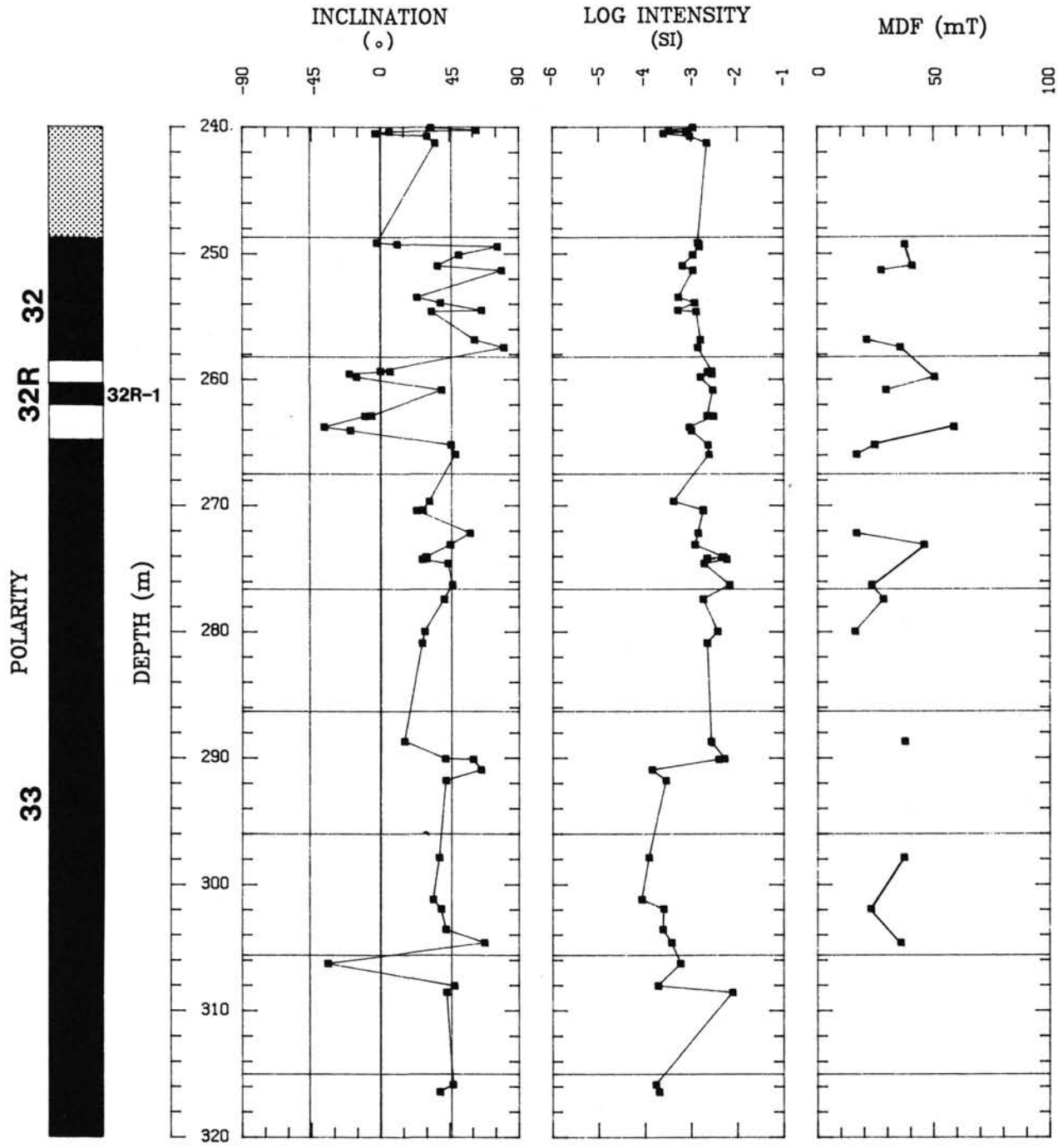

Figure 5. Magnetic parameters and magnetostratigraphic interpretation of Campanian chalk samples from Hole 627B plotted vs. depth. Box on far left shows interpreted magnetic polarity. Black indicates normal polarity, no shading denotes reversed polarity, and stippled pattern represents gaps in the record or indeterminate polarity. Bold numbers label the magnetic-polarity chrons (from time scale of Harland et al., 1982). Also plotted are inclination of the characteristic remanent magnetization (negative to the left), logarithm of NRM intensity (in Amperes/meter), and MDF (in milliTeslas). On the inclination plot, the three vertical lines are zero, and the negative and positive geocentric axial dipole indicates inclination of the site. Horizontal lines on the inclination, intensity, and MDF plots show the breaks between cores.

constrained Oligocene section in Cores 101-628A-16H to -30X. The sediments in Cores 101-628A-16H to -24X were deposited during the middle to late Oligocene at a rate of about 12–27 m/m.y., whereas those in Cores 101-628A-25X to -30X were laid down during the early Oligocene at a rate of approximately 9–10 m/m.y. (Austin, Schlager, et al., 1986). Unfortunately, two factors made reliable magnetic-polarity interpretations difficult. First, the NRM intensities and MDFs of most samples were low (Fig. 9). Consequently, many samples were too weakly magnetic to be accurately measured after AF demagnetization. Furthermore, even if the magnetizations were measured accurately, the low MDFs indicate that the magnetic vector measured may not be geologically significant for some samples. Second, gaps in the polarity record occurred owing to poor recovery in some cores, particularly near the bottom of the hole.

Figure 9 shows a plausible magnetostratigraphic interpretation of Cores 101-628A-15H to -25X that is consistent with microfossil identifications reported in Austin, Schlager, et al. (1986).

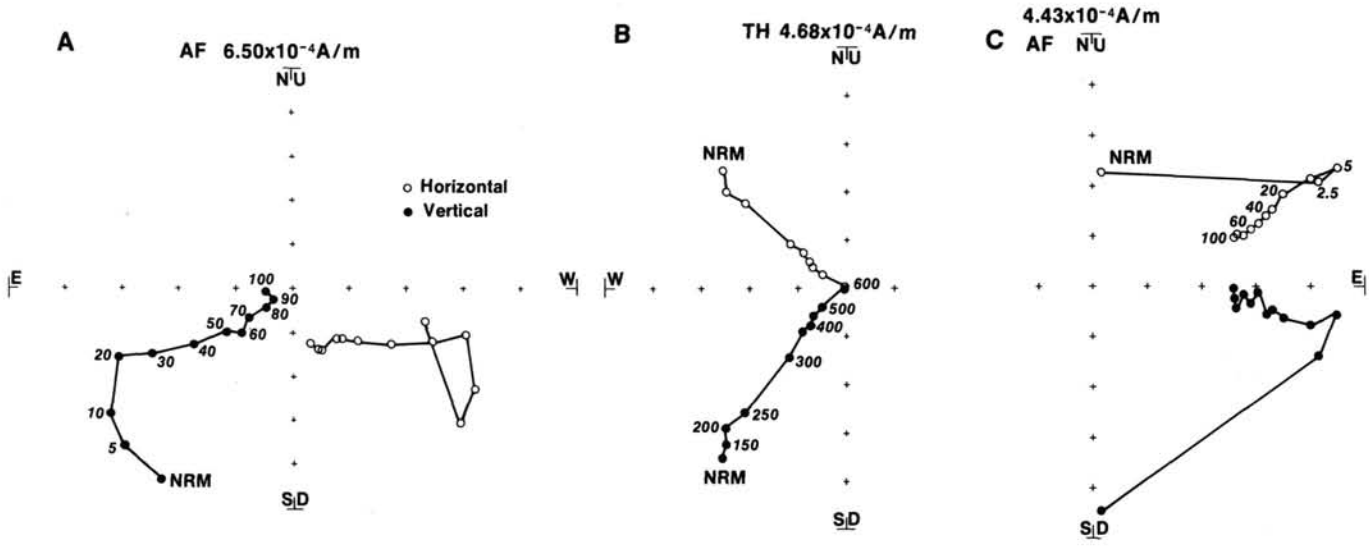

Figure 6. Orthogonal vector plots of demagnetization curves for chalk samples from Holes 627B and 634A. *A* shows the AF demagnetization of Sample 101-627B-27X-2, 75 cm, showing an overprint that is removed by a field of 20 mT. A thermal demagnetization of a similar sample, 101-627B-34X-5, 104 cm, from the same Campanian-age section is shown in *B*. The behavior of these two samples is typical of others in the same unit. An AF demagnetization of a high coercivity chalk sample, 101-634A-2R-1, 121 cm, is shown in *C*. Conventions as in Figure 2.

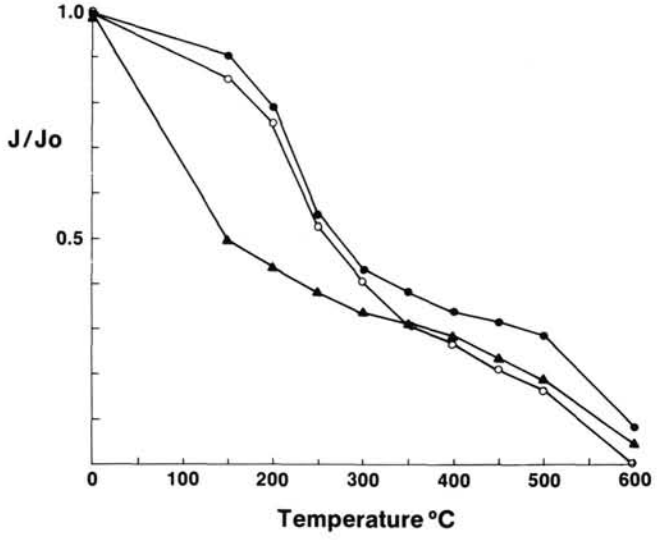

Figure 7. Plot of normalized magnetization intensity vs. temperature for samples from the Campanian chalk unit of Hole 627B. Solid dot, 101-627B-33X, CC (40 cm); open dot, 101-627B-34X-6, 78 cm; triangle, 101-627B-29X-5, 55 cm.

As shown in the figure, the inclinations are scattered, and although sections of normal and reversed polarity can be recognized, it is difficult to precisely define polarity boundaries. Recovery in Cores 101-628A-16H to -19H was good, and within this interval were found three subsections in which the samples yielded predominantly positive inclinations (i.e., normal polarity) and two shorter ones in which the inclinations were predominantly negative (i.e., reversed polarity). The reversed polarity intervals were between about 146 and 149 mbsf (Samples 101-628A-17H-1, 50 cm, to -628A-17H-2, 130 cm) and 161 to 165 mbsf (Samples 628A-18H-4, 80 cm, to 628A-19H-1, 70 cm). Although this pattern could be compared to several other parts of the Oligocene geomagnetic reversal sequence, it fits relatively well that beginning at Chron 8 and ending at Chron 9. These polarity intervals occurred during the Chattian Stage of the late Oligocene (Berggren et al., 1985). If this interpretation is correct, the reversals are Chron 8r and Subchron 9-1r (Harland et al., 1982).

The polarity record is even more difficult to follow below the top of Core 101-628A-19H owing to poor recovery. Core 101-628A-20H returned empty, Core 101-628A-19H was only 60% full, and recovery in Cores 101-628A-21H, -24X, and -25X was 50% or less. On the basis of polarity interpretation of Cores 101-628A-16H through -19H, the normal polarity samples in this section are tentatively correlated to Chrons 10 and 11, whereas the reversed polarity samples are thought to represent Chron 10R (Fig. 9).

Hole 633A, Plio-Pleistocene Section

Periplatform oozes from the upper eight cores of Hole 633A proved to be excellent material for magnetostratigraphic study for a number of reasons. First, recovery in Cores 101-633A-1H to -7H was excellent, ranging from 92% to 100%. Second, the NRM intensities and MDFs of the samples were greater than those of most others measured in this study. Third, these sediments were deposited uniformly at rates of 10 to 28 m/m.y., with few turbidites and only one significant hiatus (Austin, Schlager, et al., 1986). Finally, biostratigraphic and oxygen-isotope age control in these cores is excellent (Droxler et al., this volume).

One interpretation of the magnetostratigraphy of Cores 101-633A-1H to -8H is shown in Figure 10. The upper 43.8 mbsf of these sediments can be easily interpreted. With one exception, all samples from Cores 101-633A-1H and -2H are normally polarized and correspond to the Brunhes Chron. The reversed sample, at 8 mbsf, occurs at the boundary between the first and second core and thus is probably the result of coring disturbance. The boundary between the Brunhes normal and Matuyama reversed chrons appears at the break between the second and third cores, at a depth of 18.3 mbsf. A short normal polarity subchron, probably corresponding to the Jaramillo event, is seen at 19.9 mbsf. Although the Jaramillo is represented by only one normal polarity sample, 101-633A-3H-2, 10 cm, the sample below it, 101-633A-3H-2, 50 cm, has an inclination that appears to be transitional between normal and reversed polarity.

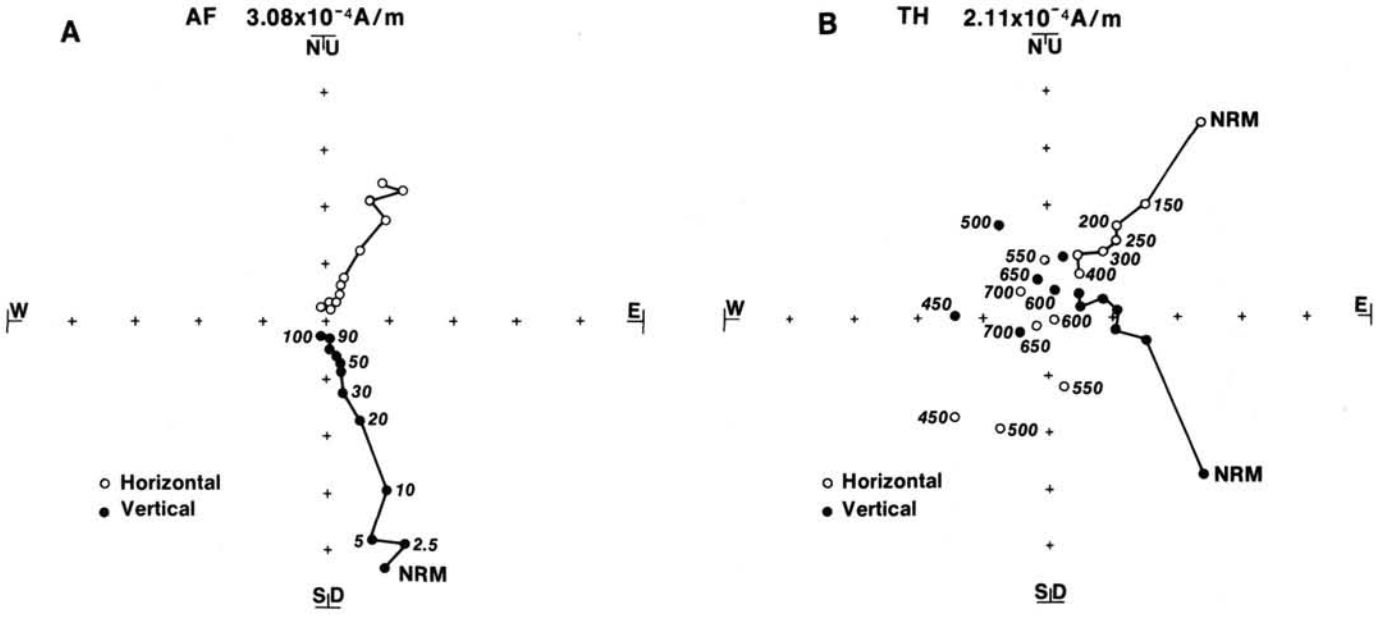

Figure 8. Orthogonal vector plots of demagnetization curves from samples of the chalky limestone unit of Hole 627B. *A*, AF demagnetization, Sample 101-627B-39X-2, 112 cm; *B*, thermal demagnetization, Sample 101-627B-41X-7, 14 cm. Note that magnetization of the sample in *B* becomes unstable when heated above 400°C. Conventions as in Figure 2.

The rest of Core 101-633A-3H and all of Core 101-633A-4H yielded reversely polarized samples that evidently record the younger half of the Matuyama Chron. However, at depths of 39.5 to 41.8 mbsf in Core 101-633A-5H are samples with normal polarity. Two lines of evidence imply that this is the Olduvai Subchron. First, its depth is consistent with its proposed age (1.67–1.87 Ma, Harland et al., 1982) and the sedimentation rate extrapolated from the depths of the Brunhes/Matuyama boundary and the Jaramillo Subchron. Second, calcareous nannofossils from this level of the hole have an age consistent with that of the Olduvai Subchron (Droxler et al., this volume).

An interesting aspect of the magnetostratigraphy of the sediments above the Olduvai Subchron is the lack of certain reversals that have been reported within the Brunhes and the latter half of the Matuyama. Six or seven short excursions or reversals (Starno, Laschamp, Mono, Blake, Biwa I and II, and Emperor), lasting for periods on the order of 1.0×10^4 yr or less, have been recognized within the Brunhes by various authors (Verosub and Banerjee, 1977; Champion et al., 1981; Tarling, 1983). However, no obvious events are seen within the Brunhes in the inclination record shown in Figure 10. Both the sedimentation rate and the sample spacing, however, make it difficult to identify such short events. Each sample spans 2 cm of depth, and the samples within the Brunhes are spaced 0.5 m apart. Thus the paleofield measurements are separated by approximately 2.1×10^4 yr, and each sample averages the field over a period of about 800 yr. Nonetheless, it is somewhat surprising, given the number of such events that have been hypothesized, that there is no evidence of any event within the Brunhes in these cores.

At least one reversal with a duration thought by some to approximate that of the Jaramillo is conspicuously absent. It is the Gilsa normal polarity subchron, which may have occurred within the Matuyama Chron about 0.2 m.y. prior to the Olduvai Subchron (McDougall, 1979). Although there appears to be a consistent shallowing of the inclination slightly above the Olduvai (Fig. 10), the Gilsa is not evident. Notably, this subchron is not included in many time scales (e.g., Harland et al., 1982; Berggren et al., 1985). This event probably had a short duration and was missed as a result of the coarse sampling interval used in this study. A recent high-resolution study of the magnetostratigraphy of DSDP Hole 609 in the North Atlantic by Clement and Kent (1987) suggests that the Gilsa was indeed very short and may have only been an excursion, not a true reversal.

Below the Olduvai, magnetostratigraphic interpretation is somewhat more difficult because fewer samples per core were taken deeper than 40 mbsf. Furthermore, these samples have lesser NRM intensities and generally lower MDFs than those above. A gap in the calcareous-nannofossil stratigraphy occurs at a depth of 43.75 mbsf (Droxler et al., this volume). Only two samples were obtained above the hiatus and below the Olduvai Subchron. One is reversed and probably represents the reversed field of the Matuyama Chron just prior to the beginning of the Olduvai. The other, at a depth of 43.3 mbsf, has normal polarity and may have acquired its magnetization during one of the short normal polarity Reunion events that occurred between 2.01–2.04 and 2.12–2.14 Ma (Harland et al., 1982).

The samples directly below the hiatus show negative inclinations, implying reversed polarity. Given the constraint of the nannofossil stratigraphy, they probably represent the Gilbert reversed chron. The normal zones at depths of 47.0–48.8 mbsf, 49.5–50.9 mbsf, 55.6–58.5 mbsf, and 60.8–71.8 mbsf are interpreted as the Cochiti, Nunivak, Sidufjall, and Thvera subchrons within the Gilbert Chron (Harland et al., 1982).

DIAGENESIS OF STRONGLY MAGNETIC CARBONATE OOZES

Several holes drilled during Leg 101 yielded carbonate ooze at shallow sub-bottom depths with high magnetic intensities that systematically decreased downhole by two to three orders of magnitude. This was most noticeable in Holes 632A and 633A (Fig. 11). Sediments from these two holes had NRMs as high as 10^{-2} A/m in the upper few meters below the seafloor. In both cases, the NRM intensity remained between 10^{-2} and 10^{-3} A/m for the first 7 to 8 mbsf, but subsequently it began an exponential decrease to about 10^{-4} to 10^{-5} A/m at depths of 17–18 mbsf (Fig. 11). Magnetic-susceptibility values in each hole mimic the NRM intensities (Austin, Schlager, et al., 1986).

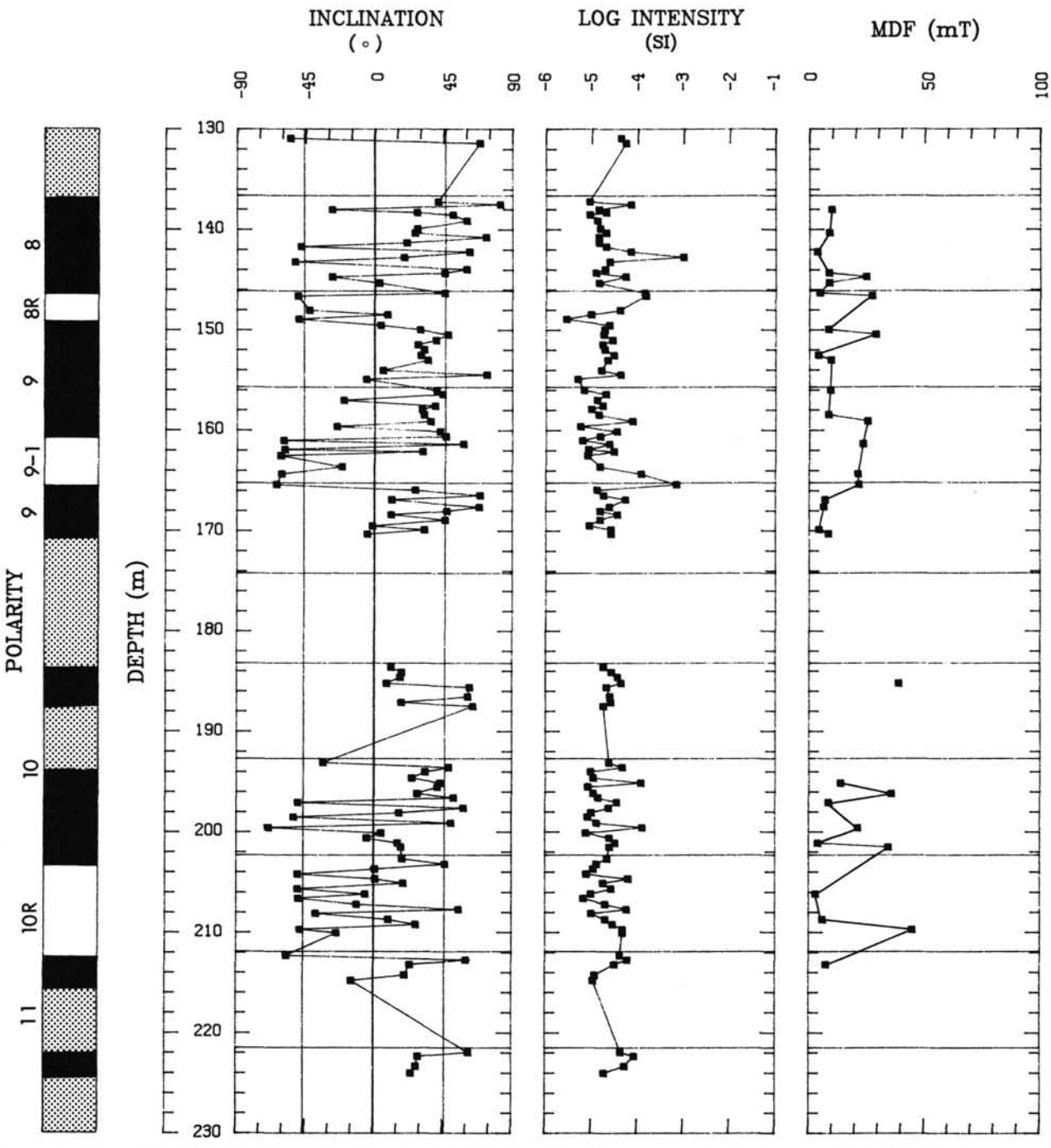

Figure 9. Plot of magnetic parameters and polarity interpretation, mid-Oligocene section of Hole 628A. Conventions as in Figure 5.

Similar behavior was noted in cores from Hole 627B, but the NRM decay occurred over an interval of only about 5 m (Fig. 11). No such phenomenon was noted in sediments from Hole 628A or Hole 631A, although NRM intensities as high as 10^{-3} A/m were measured between 6 and 9 mbsf in Hole 631A (Fig. 11).

An interesting aspect of these observations is the high-intensity magnetization of sediments from Holes 632A and 633A. These two holes, along with Hole 631A, are in the southern part of Exuma Sound. This sound is deep and surrounded by carbonate banks and has restricted access to the Atlantic Ocean. Its entrance faces east, away from sources of continental sediments, and is blocked from general ocean circulation by several islands and the Antilles Current, which sweeps along the eastern boundary of the Bahamas. Consequently, continental detritus, commonly thought to be a major source of magnetic minerals in sediments, should not be found in this basin in large quantities. Nevertheless, the sediments near the seafloor are strongly magnetic.

One possible explanation of this paradox is that the carrier of the magnetic remanence is biogenic magnetite. In recent years researchers have found, in sediments of various ages and locales, pseudo-single-domain magnetite grains formed by magnetotactic bacteria or algae near the seafloor (Kirschvink, 1982; Kirschvink and Chang, 1984; Petersen et al., 1986; Stolz et al., 1986). Moreover, others have hypothesized that similar magne-

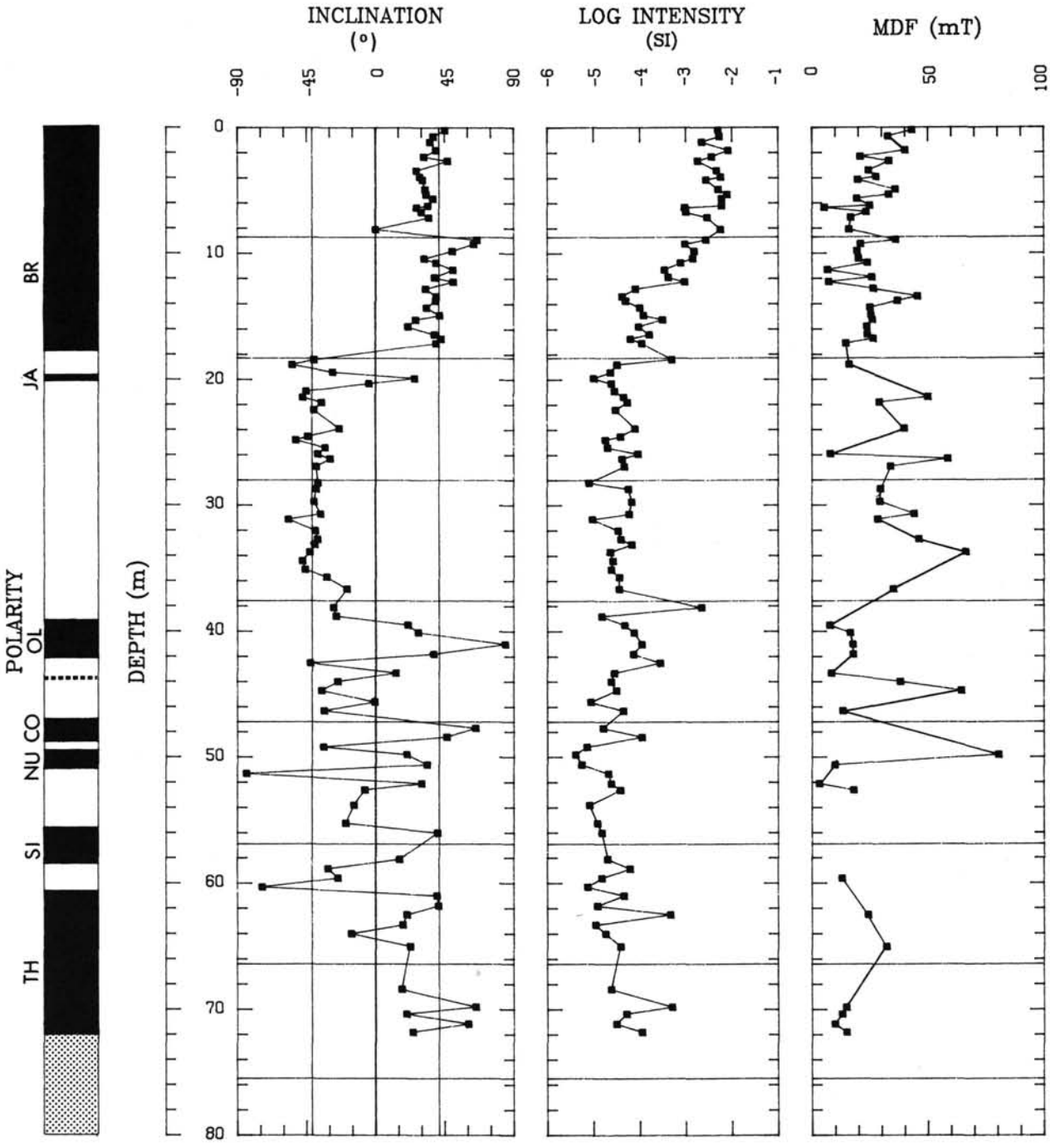

Figure 10. Plot of magnetic parameters and polarity interpretation, Plio-Pleistocene section of Hole 633A. Conventions as in Figure 5. Dashed line in the polarity column represents a hiatus as reported by Droxler et al. (this volume). Subchrons: TH = Thvera; SI = Siduf-jall; NU = Nunivak; CO = Cochiti; OL = Olduvai; JA = Jaramillo. BR = Brunhes Chron.

tite can be formed by microaerophilic microbes within the sediment column (Karlin et al., 1987) or even by teeth grown by chiton (Kirshvink and Lowenstam, 1979). Indeed, this explanation of the high magnetic intensities seems likely because bacterial magnetosomes have recently been reported in sediments drilled on San Salvador Island, near the mouth of Exuma Sound (McNeil et al., 1987).

Demagnetization pilot studies yielded further evidence that magnetite grains carry the remanent magnetism of the sediments in the upper parts of Holes 632A and 633A. Unlike most of the carbonate-ooze samples, those from just below the seafloor in these holes displayed a stable magnetization and univectorial decay when heated (Fig. 12). Furthermore, upon heating they retained a significant portion of their remanence up to a temperature of 550°C but were completely demagnetized by 600°C (Fig. 13). In addition, these sediments also showed stable behavior during AF demagnetization and yielded moderately high MDFs. All of these properties are characteristic of fine-grained magnetite.

The rapid magnetic-intensity decrease with depth below seafloor in Holes 627B, 632A, and 633A resembles that attributed by other researchers to the diagenetic reduction of magnetic minerals. Although other phenomena could account for the observed trends, the data appear most consistent with the effects

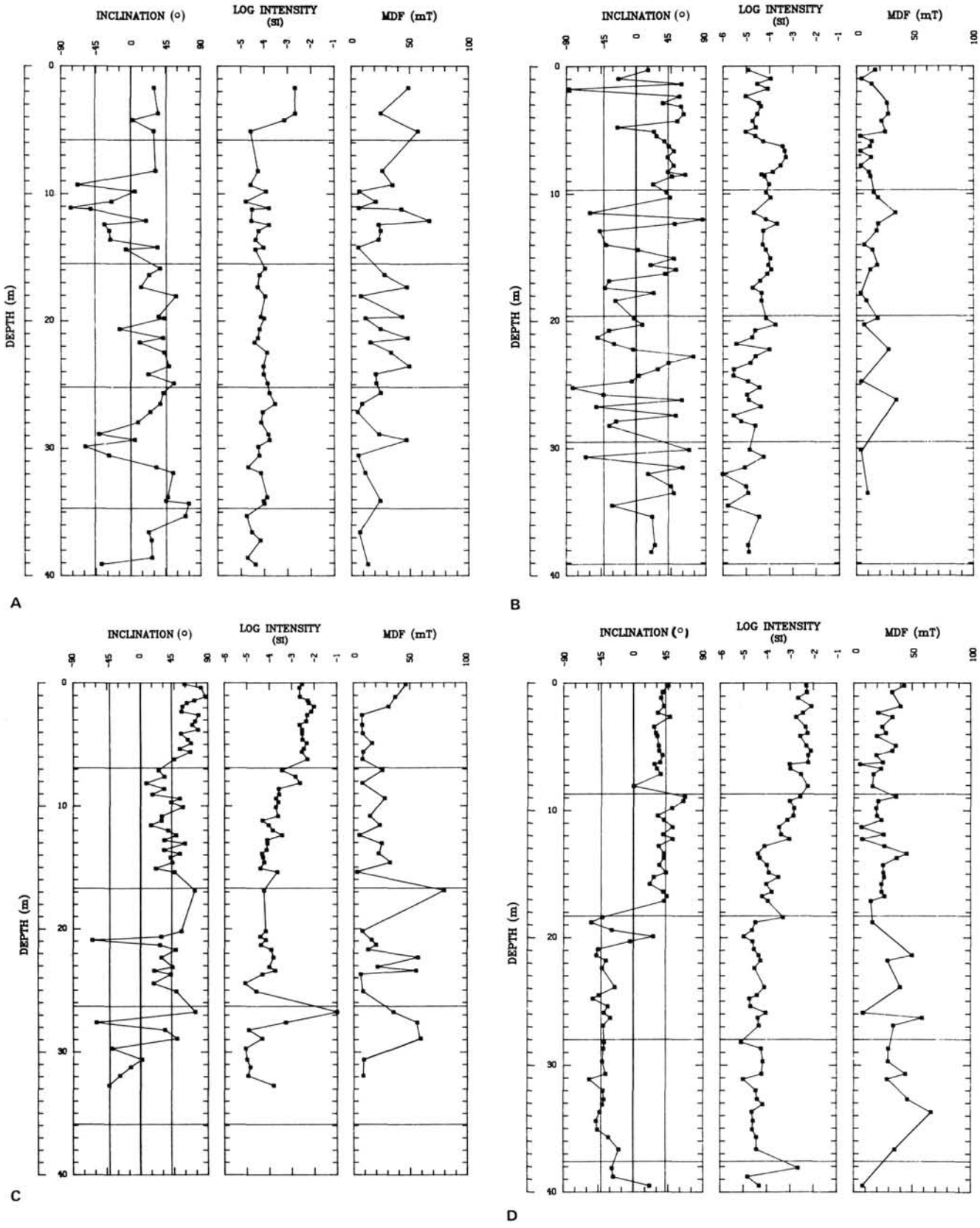

Figure 11. Magnetic parameters for the upper 40 mbsf of Holes 627B (*A*), 631A (*B*), 632A (*C*), and 633A (*D*), showing high magnetic intensities and decay of NRMs. Hole 627B is north of Little Bahama Bank, whereas the other three are in Exuma Sound. Conventions as in Figure 5.

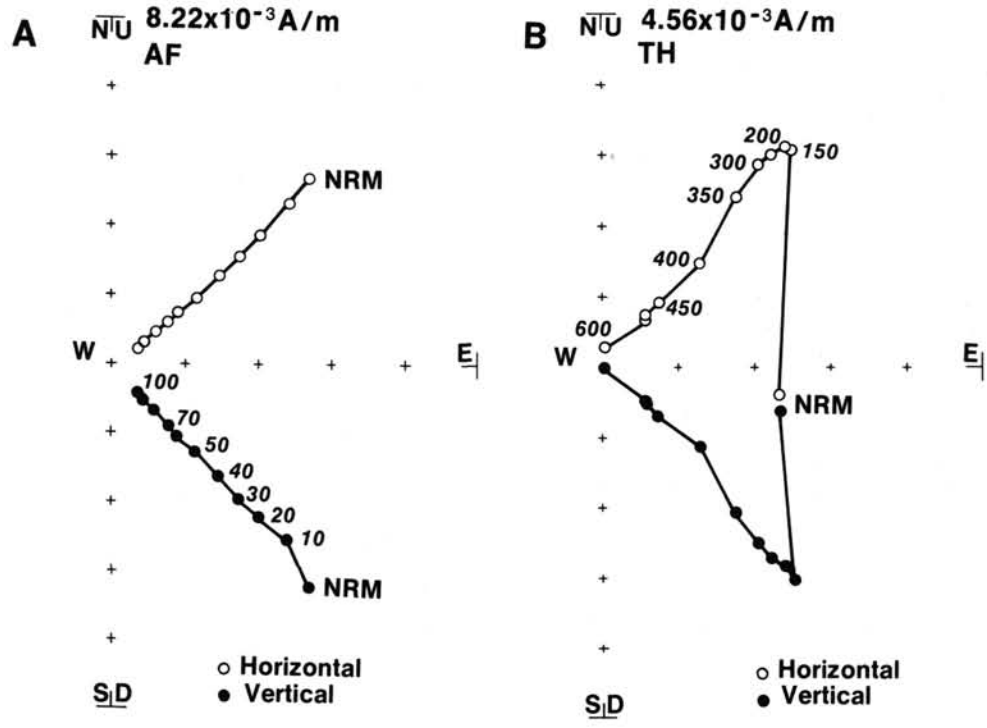

Figure 12. Orthogonal vector plots of demagnetization curves for samples from the high NRM section of Hole 633A. *A*, AF demagnetization, Sample 101-633A-1H-2, 30 cm; *B*, thermal demagnetization, Sample 101-633A-1H-1, 114 cm. Conventions as in Figure 2.

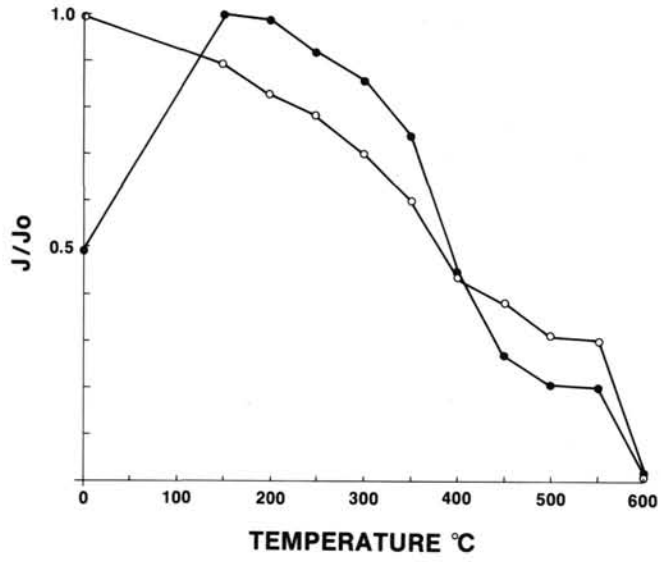

Figure 13. Plot of normalized magnetic intensity vs. temperature for samples from the strongly magnetic sections of Holes 632A and 633A. Open dot, Sample 101-632A-1H-1, 40 cm; solid dot, Sample 101-633A-1H-1, 114 cm.

of diagenesis. Alterations in paleoenvironment or paleocurrents, for instance, might have changed the amount of magnetic material being deposited. Nonetheless, the decrease of NRM intensities and susceptibility does not appear to have resulted from dilution of the magnetic minerals. In Hole 633A, for example, Droxler et al. (this volume) constructed a detailed profile of the percentage of carbonate in the same sediments that show the decrease in magnetism. Although variations appear, they are small and do not correlate with the variation in the magnetic properties. Additionally, the few carbonate-bomb data taken in the upper few cores of Holes 627B and 632B during Leg 101 (Austin, Schlager, et al., 1986) show no obvious systematic increase in the carbonate percentage with depth that might cause the observed trend in magnetic properties.

The decrease in magnetism also appears to be controlled by the depth of the sediments rather than by their age. In Hole 633A, the NRM intensities reach their lowest level at a depth of about 18 to 19 mbsf near the Brunhes/Matuyama polarity chron boundary (Figs. 10 and 11). In nearby Hole 632A, the NRM intensity reaches its base level at about the same depth. It appears that the Brunhes/Matuyama boundary is about twice as deep in this hole than it is in Hole 633A. These observations imply that the pattern of magnetism was probably not caused by an environmental change that would have affected both locales simultaneously. Instead, most of the geochemical and magnetic parameters point to diagenetic dissolution of the magnetic minerals as the cause of the downhole variation.

Magnetite and other iron oxides are progressively reduced and subsequently sulfidized and pyritized with burial in suboxic or anoxic-sulfidic environments (Karlin and Levi, 1983, 1985; Leslie et al., 1984). The ultimate cause of the diagenesis is decomposition of organic matter by microbial oxidation. If sufficient organic matter is present, sulfate reduction occurs and reduced iron in the porewater becomes sulfidized, initially forming metastable monosulfides and eventually nonmagnetic pyrite (Karlin and Levi, 1983).

Most of the conditions necessary for these reactions are found in Holes 627B, 632A, and 633A (see Austin, Schlager, et al., 1986). Organic matter is present in the uppermost cores in sufficient quantities to create a suboxic or anoxic-sulfidic depositional environment. Sulfate concentration decreases downhole, and pyrite is a common accessory mineral, indicating that sulfidization has occurred.

Although the diagenetic dissolution of the magnetic minerals observed in Leg 101 holes is similar to that observed in sediments elsewhere, there are some interesting differences. The plot of NRM vs. depth (Fig. 11) has a shape similar to those in the literature (e.g., Karlin and Levi, 1985), but occurs over a larger depth range. Whereas hemipelagic sediments near the continental margins have NRMs that are greatly reduced in the upper few tens of centimeters (Karlin and Levi, 1983, 1985), the same type of decrease occurs over a depth of 5 m in Hole 627B and 18–19 m in Holes 632A and 633A. This difference probably reflects the amount and reactivity of the organic matter as well as the efficiency of the microbial chemical reactions.

Another divergence from the expected pattern occurs in the MDF values. In published accounts of this reduction phenomenon (Karlin and Levi, 1983), the MDF values mimic the NRM values and decrease downcore at about the same rate. The lessening of MDFs is attributed to the dissolution of the finer fraction of magnetic minerals, which are the most magnetically stable and resistant to AF demagnetization. In Hole 627B the MDF values are rather variable and scarce in the section of interest, so it is difficult to draw conclusions. However, in both Holes 632A and 633A, the MDFs decrease much more rapidly than does NRM intensity (Fig. 11). For example, the MDFs in Hole 632A drop from near 50 mT to below 10 mT within the first few meters below seafloor, whereas those in Hole 633A decline more gradually from near 50 mT to values predominantly between 20 and 30 mT within 7 m of the seafloor. The rapid decrease of MDFs, as opposed to the slower decline of the NRM intensities, might be the result of an uneven distribution of magnetic minerals, in which small amounts of fine, stable grains are quickly dissolved and the larger, more abundant, somewhat less stable grains endure. Curiously, the MDF values in both holes appear to rise gradually over the next several tens of meters downhole. Perhaps another magnetic mineral, possibly one of the metastable iron sulfides such as greigite or pyrrhotite, is precipitated along with the pyrite as the reduction reactions progress. This hypothesis might also explain why the highly magnetized carbonate-ooze samples from near the seafloor can be thermally demagnetized, whereas the weaker oozes farther downhole exhibit unstable behavior when heated. Experiments on naturally occurring greigite, for instance, have shown that greigite alters to other minerals when heated at relatively low temperatures (Reynolds et al., 1986).

Another interesting phenomenon is the difference in magnetic patterns among the three holes drilled in Exuma Sound. Holes 632A and 633A give similar results, but 631A looks very different (Fig. 11). Unlike the other two holes, Hole 631A shows no evidence of a layer of strongly magnetic sediments near the seafloor. Furthermore, although no sediments in 631A have NRM intensities as high as those in the other holes, a zone of ooze with NRM intensities near 10^{-3} A/m appears between 6 and 9 mbsf. In addition, the MDFs are generally low and show no obvious pattern. Because the geochemical environment in all three holes is similar, it is unclear why the results from Hole 631A are so different from those measured in other holes in the same basin. The divergence may be related to water depth (Hole 631A is the shallowest, at 1081 m water depth, whereas 632A and 633A are at 1996 and 1681 m), or it may be caused by differences in the input of magnetic material or the rate of its dissolution. A more intensive geochemical and rock-magnetic study is required to sort out the complex chemical interactions occurring in these holes.

PALEOLATITUDES

Paleolatitudes were calculated from samples of various ages from Leg 101 cores for comparison with site latitudes and published paleomagnetic data from the North American plate. Because none of the cores were azimuthally oriented, it is impossible to determine the direction of the paleomagnetic pole (i.e., the true declination). The inclination data constrain the location of the paleomagnetic pole to a small circle centered on the sampling location. Special statistics must be used to calculate unbiased estimates of the mean inclination. Several authors have developed methods for making such calculations (Kono, 1980; McFadden and Reid, 1982; Cox and Gordon, 1984), all of which give similar results at low latitudes. The algorithm developed by Kono (1980) was used in this study for the computation of mean inclinations, paleolatitudes, and their error limits.

The paleomagnetic measurements (Appendix) were divided into time units using biostratigraphic ages (Austin, Schlager, et al., 1986) and the time scales of Berggren et al. (1985) and Kent and Gradstein (1985). An attempt was made to split the measurements into the smallest possible time units, and at least 10 samples were used to compute each mean paleolatitude. Histograms of inclination values were then constructed for each time unit to examine the distribution of the data and expunge outlier values from the analysis. In addition, mean inclinations with a Fisherian precision parameter, k, of less than 10 were considered to be unreliable. Results of these inclination and paleolatitude calculations are given in Table 1.

In general, the weakly magnetic ooze samples gave the poorest results with the most scatter, whereas the more strongly magnetic samples, particularly those from the upper four cores of Hole 633A, gave the best. This result is not surprising, given the MDF characteristics (Fig. 2) of these sediments. Figure 14 shows inclination histograms representative of both types of results. The Campanian chalk samples and the Cenomanian chalky-limestone samples from Hole 627B also yielded good results; in both the success of the calculations is partly due to the large number of samples available from each unit and to their relatively strong and stable magnetizations. These are particularly important because they correspond to periods of time during which paleomagnetic data from the North American plate display significant apparent polar wander.

To compare the results from various sites, a quantity, D, the observed paleolatitude minus the present site latitude, was plotted (Figs. 15 and 16). Negative D, for example, implies that the site is north of its paleolatitude. North and south shifts in latitude, as reflected by paleomagnetic data, are often attributed to tectonic motion. However, other geophysical phenomena, true polar wander (Jurdy, 1981; Andrews, 1985), and persistent nondipole geomagnetic-field components (Wilson, 1971; Merrill and McElhinny, 1977; Coupland and Van der Voo, 1980; Livermore et al., 1983, 1984) can also give rise to apparent latitudinal shifts. Likewise, systematic errors in the paleolatitude data, such as off-vertical tilt of the drill hole or biased magnetic-field recording properties of the sediments (e.g., "inclination error") can also cause latitude anomalies.

In Figure 15 most of the paleolatitudes less than 10 Ma appear statistically indistinguishable from zero. However, three data, the 1.2-Ma paleolatitude from Hole 627B and two paleolatitudes from Hole 633A, 0.17 and 4.3 Ma, are exceptions. In each case the paleolatitude is south of the present latitude. It is surprising that any of the paleolatitudes are different from zero, because the northward component of the tectonic drift of the North American plate, upon which the Bahamas rest, has been small during the last 10 m.y. (Klitgord and Schouten, 1986). Consequently, it is tempting to dismiss the anomalous data as inaccurate. In the case of the 1.2-Ma datum from Hole 627B, this assumption may be correct, as the inclinations used to calculate this paleolatitude show considerable scatter; this is not true for the anomalous data from Hole 633A.

The southward position of these two points cannot be easily ascribed to off-vertical tilt of the hole or to inclination error, because three other paleolatitudes from the same hole are close to

Table 1. Paleolatitudes calculated from ODP Leg 101 sediments.

Hole	Latitude (°N)	Longitude (°W)	Cores	Paleolatitude (°N)	95% Confidence	D	k	N	Age (Ma)
627B	27.6	78.3	1-2	16.8	7.0	−10.8	14	13	0.6-1.8
			3-5	24.3	6.2	−3.3	13	25	2.2-4.0
			8-10	27.7	11.4	0.1	10	12	5.6-8.3
			27-34	22.7	3.6	−4.9	17	50	72-78
			37-47	30.8	3.3	3.2	15	106	93-97
628A	27.5	78.3	16-23	25.8	5.5	−1.7	12	36	27-31
631A	23.6	75.7	1	25.0	8.4	1.4	17	11	0.1-0.5
			2-3	27.9	11.4	4.3	10	13	0.5-2.2
632B	23.8	75.4	4-16	19.4	6.9	−4.4	10	20	5.6-8.3
633A	23.7	75.6	1	19.3	2.3	−4.4	112	15	0-0.35
			2	23.6	5.0	−0.1	29	16	0.35-0.73
			3	22.1	4.6	−1.6	37	14	0.73-1.4
			4	23.8	3.2	0.1	94	12	1.4-1.8
			5-8	16.7	4.9	−7.0	13	27	4.0-4.6
634A	25.4	77.3	2-4	18.1	6.1	−7.3	15	17	56-58
635B	25.4	77.3	3-13	28.7	7.3	3.3	16	19	95-100

95% Confidence = half-width of 95%-confidence region, in degrees; D = site paleolatitude minus present site latitude; k = precision parameter (Fisher, 1953); N = number of samples.

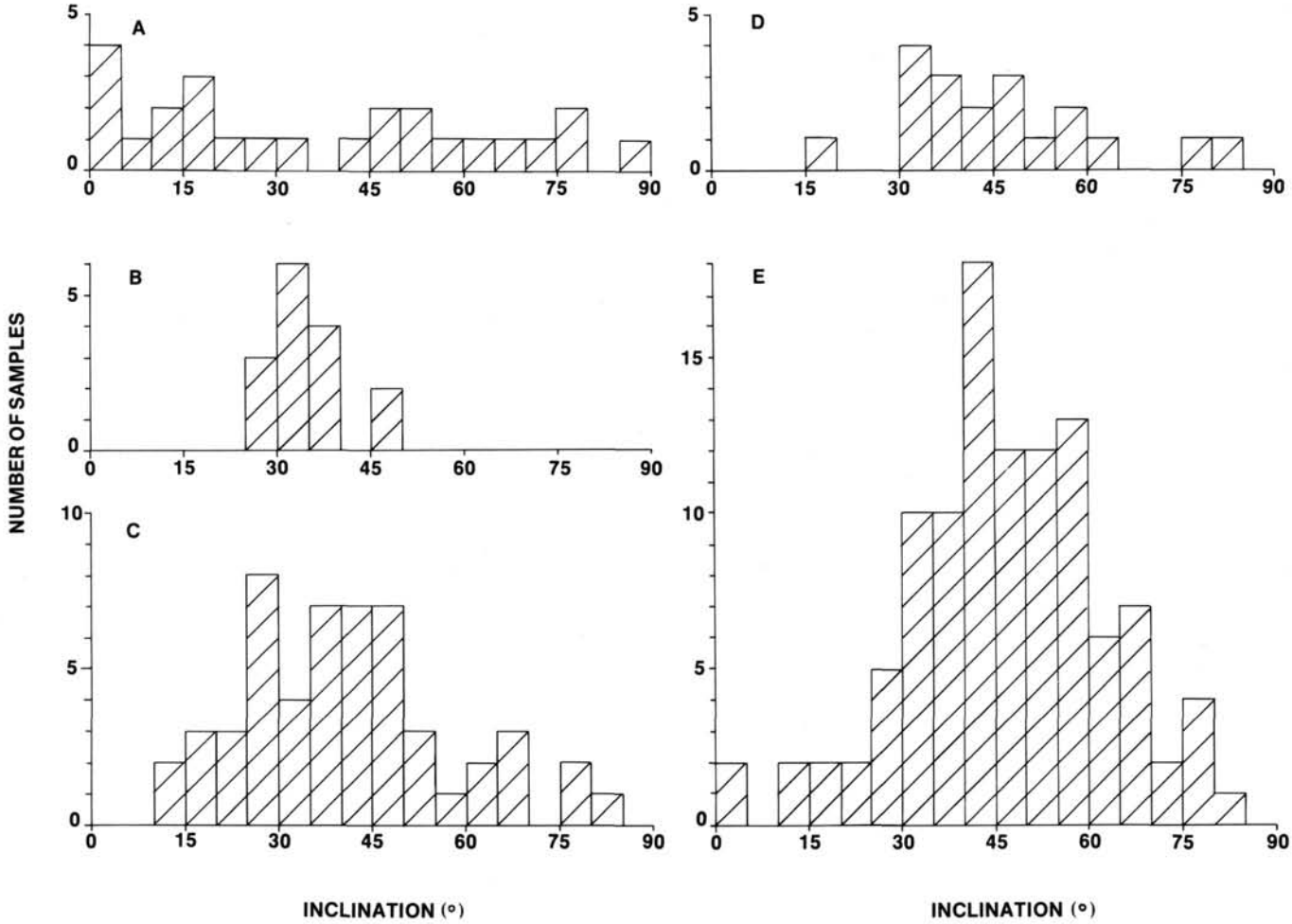

Figure 14. Histograms of inclination values from the paleolatitude calculations. *A*, large scatter typical of weakly magnetized carbonate-ooze samples from Core 101-626C-14H to -18H. *B*, clustering of inclination values in strongly magnetic carbonate-ooze samples from Core 101-633A-1H. Distribution of inclinations from Cretaceous samples: *C*, Campanian chalk unit, 101-627B-27X to -34X; *D*, Albian-Cenomanian chalky-limestone samples, 101-635B-8R, -10R to -13R; *E*, Cenomanian chalky-limestone samples, 101-627B-37X to -47X.

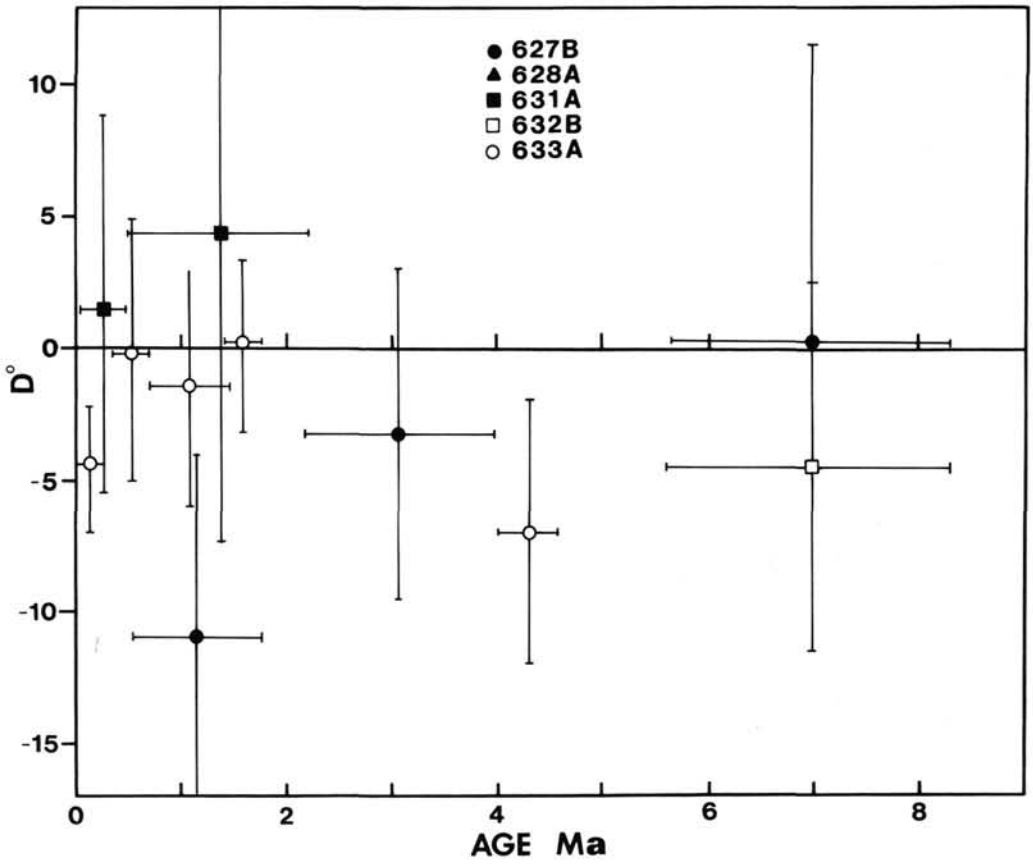

Figure 15. Plot of latitudinal change, *D* (paleolatitude minus present latitude), vs. age for 0–10 Ma. Vertical bars are the 95%-confidence limits of the paleolatitude, and horizontal bars are the range of biostratigraphic ages of the samples used to calculate the paleolatitude.

zero, as expected. True polar wander also does not appear to be a good explanation of the anomalous data for two reasons. First, these data imply rates of true polar wander, 3° to 20°/m.y., much higher than generally accepted values (e.g., Andrews, 1985). Second, many recent studies of true polar wander have concluded that it was insignificant during the late Tertiary (Livermore et al., 1983, 1984; Sager, 1984).

Long-term nondipole fields do, however, seem to be a plausible explanation of these data. Several researchers have found evidence of nondipole fields in the late Tertiary that result in "far-sided" paleomagnetic poles (e.g., Wilson, 1971; Merrill and McElhinny, 1977). Furthermore, this bias appears to increase rapidly with increasing age in the last 20 m.y. (Epp et al., 1983). A far-sided effect should cause negative values of the quantity *D*, perhaps explaining the 4.3-Ma datum and the generally negative *D* values prior to 2 Ma in Figure 15. The anomalous 0.17 Ma paleolatitude may be the result of the failure of the geomagnetic field to average into a geocentric axial dipole in the last few tens of thousands of years. A similar phenomenon has been noted in paleomagnetic data from recent Hawaiian Island lavas (Coe et al., 1978).

Nondipole fields probably also have had an effect on Late Cretaceous and early Tertiary paleolatitudes, but because of the greater span of time involved, the same is true of tectonic motion and true polar wander. With the limited amount of data analyzed in this study it was impossible to sort out these various phenomena with any reliability. However, the paleolatitudes of these ages from this study mostly agree with values expected from tectonic-motion models and other North American plate paleomagnetic data (Fig. 16). The one possible exception is a datum from the Cenomanian chalky-limestone unit of Hole 627B. Although its precision is among the best of the paleolatitudes calculated in this study (Table 1), this datum implies that the northern Bahamas were about 3° north of their present position during the Cenomanian rather than 3° and 8° south, as inferred from other North American paleomagnetic data (Harrison and Lindh, 1982), and plate motion vs. the hotspots (Morgan, 1983), respectively. As shown in Figure 16, the 95%-confidence limit of this datum overlaps that of the apparent polar-wander path, but only partly.

The reason for this discrepancy is not immediately clear. In particular, the disagreement with the North American apparent polar-wander path is puzzling. Nondipole field components and true polar wander cannot be held accountable for this discrepancy because they should have affected the Hole 627B datum by approximately the same amount as the other North American paleomagnetic data. Neither is the discrepancy a result of inclination error, for the disagreement is in the opposite sense from that expected from this phenomenon. Nor is it caused by the off-vertical tilt of the drill hole, which was measured at only 0.5° in Core 101-627B-32X, just above the Cenomanian unit. Tectonic motion is also a doubtful explanation because the difference in paleolatitude suggests a southward motion of the Bahamas with respect to North America, for which there is no geologic evidence (Klitgord and Schouten, 1986).

Figure 17 provides a clue to a possible cause of the paleolatitude discrepancy. It shows that the Cenomanian datum predicts a paleomagnetic pole closer to the sampling site than that implied by the North American plate apparent polar-wander path. The polar-wander path trends toward North America and the

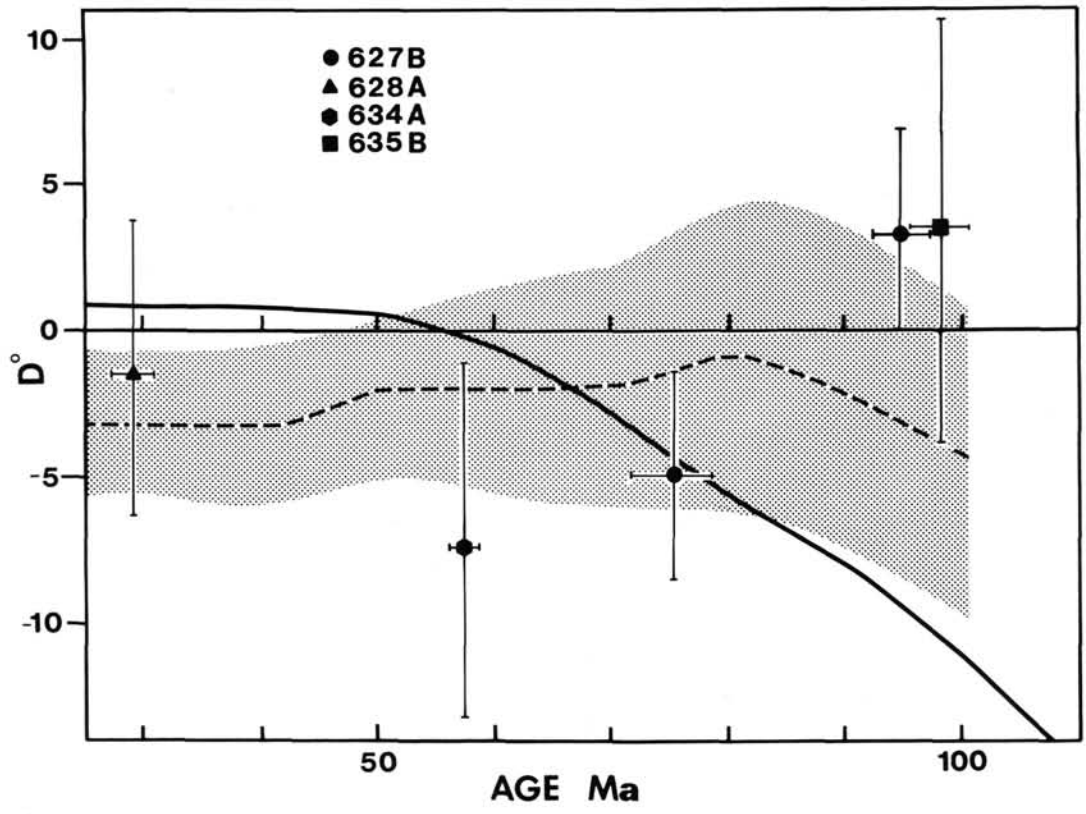

Figure 16. Plot of latitudinal change, *D*, vs. age for 25–120 Ma. Dashed line is paleolatitude shift implied by the North American plate apparent polar-wander path (Harrison and Lindh, 1982). Stippled region represents the 95%-confidence region of the polar-wander path. Solid curve is the predicted latitude shift from North American plate motion with respect to the hotspots (Morgan, 1983). Error bars as in Figure 15.

Bahamas until about 80 to 90 Ma, when it bends abruptly northward toward the geographic pole. Most published North American apparent polar-wander paths show a similar sharp bend in the mid- to Late Cretaceous. Sharp bends such as this have been interpreted as "cusps," the intersection of two segments of an apparent polar-wander path that follow small circles around Euler poles describing the motion of the plate with respect to the spin axis (Gordon et al., 1984). Typically, in calculations of poles along a polar-wander path, paleomagnetic data are averaged over 20 to 30 m.y. or more. A consequence of this averaging is that sharp features, such as cusps, are rounded. The shape of the North American apparent polar-wander path suggests a Late Cretaceous cusp pointing more or less toward North America (Fig. 17). Thus the Cenomanian datum may reflect the position of the spin axis when it was near its farthest point eastward on the cusp.

CONCLUSIONS

The intensity of magnetization in Leg 101 sediments varied by nearly six orders of magnitude, from 1.6×10^{-6} to 1.0 A/m. Most samples were weakly magnetic and had low MDF values. These samples proved only marginally useful for magnetostratigraphic and paleolatitude studies. However, several units, notably the chalk of Campanian age of Hole 627B, Cenomanian marly limestone of Hole 627B, and sediments in the upper 18–19 mbsf of Holes 632A and 633A, were more strongly magnetized and yielded more interesting paleomagnetic data. Although extensive rock-magnetic tests required to positively identify the magnetic minerals responsible for the remanence of Leg 101 samples were not undertaken, all of the results are consistent with magnetite as the primary carrier.

Magnetostratigraphic studies were done on cores from Holes 627B, 628A, and 633A. The Campanian chalk unit of Hole 627B appears to record a reversal between 259 and 265 mbsf that has been suggested to be Chron 32r. No reversals were found within the upper Cenomanian chalky limestone unit from the same hole. A mid-Oligocene section of Hole 628A with excellent biostratigraphic age control unfortunately gave poor results because of the weak magnetism of the sediments. However, Cores 101-628A-16H to -25X were tentatively correlated to Chrons 8–11. Cores from Hole 633A contained a relatively undisturbed Plio-Pleistocene sequence of sediments that yielded excellent magnetostratigraphic results. In the upper 44 mbsf of the recovered sequence, the Brunhes and Matuyama chrons were identified along with the Jaramillo and Olduvai subchrons. None of the many short polarity events hypothesized to have occurred during this time interval were detected. From 44 to 77 mbsf, the polarity stratigraphy was correlated with the Gilbert reversed chron and the Cochiti, Nunivak, Sidjufall, and Thvera subchrons.

In sediments from Holes 627B, 632B, and 633A, NRM intensities as high as 10^{-2} A/m, strong for carbonate-rich sediments, were noted near the seafloor. The NRMs declined rapidly downhole in each case. In Hole 627B, the high intensities were only recorded for about 5 mbsf, but in both Holes 632A and 633A the high values were found 18 to 19 mbsf. The magnetic properties of these sediments and the manner in which the high magnetizations decrease with depth suggest that the magnetic minerals are being dissolved by diagenesis in a suboxic or anoxic-sulfidic environment.

Paleolatitudes were determined for various time units based on biostratigraphic and magnetostratigraphic dates. Most of

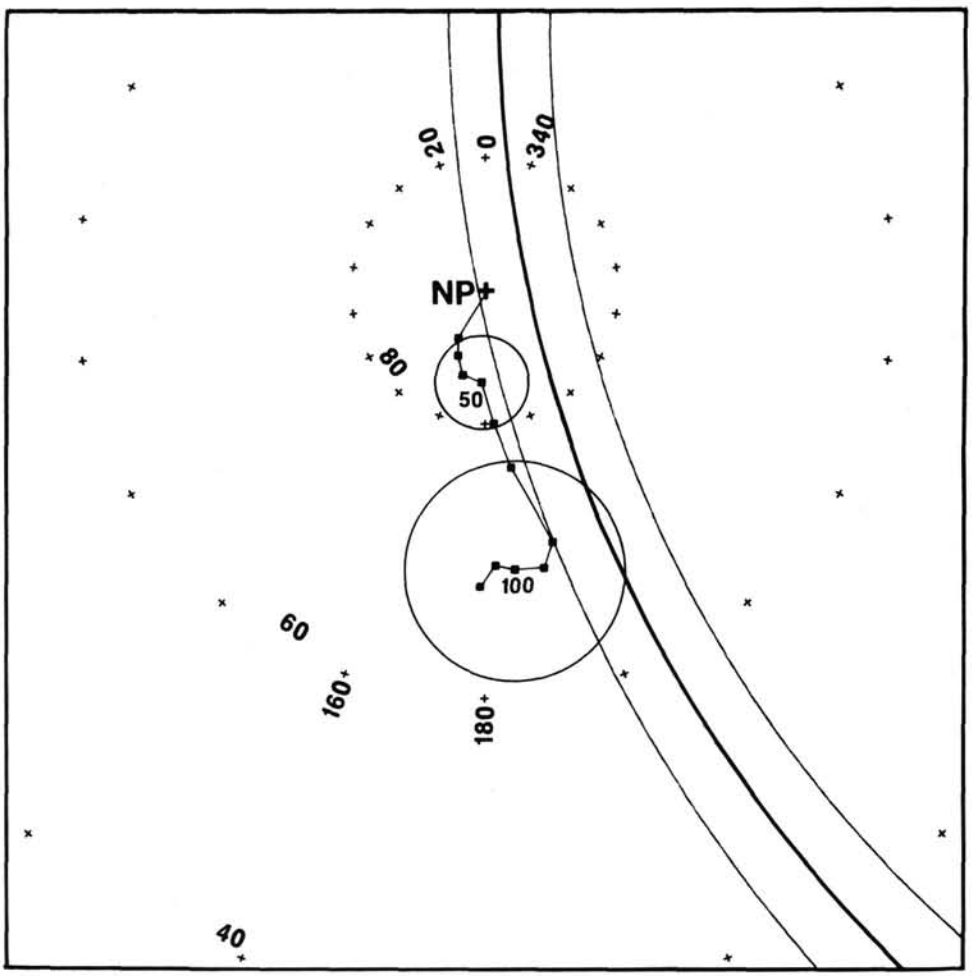

Figure 17. Comparison of polar circle calculated from the Cenomanian paleolatitude of Cores 101-627B-37X to -47X with the North American plate polar-wander path. Polar-wander path is shown by dots representing poles at 10-m.y. intervals from 20 to 120 Ma. The 95%-confidence circles shown are for 50 and 100 Ma poles. Heavy arc is polar circle, and flanking lighter arcs bound 95%-confidence annulus.

these data are not significantly different from the present latitude of the sampling sites. However, two well-determined paleolatitudes from Hole 633A suggest that small far-sided nondipole effects may have existed briefly during the last 4 m.y. Additionally, a relatively well-determined paleolatitude from the Cenomanian chalky-limestone unit of Hole 627B displays a discrepancy of 7° to 13° with respect to the expected value implied by the apparent polar-wander path of the North American plate and a model of the motion of that plate with respect to the hotspots.

ACKNOWLEDGMENTS

I thank Wulf A. Gose for the use of his paleomagnetic laboratory and JOI-USSAC for financially supporting this research. My gratitude is extended to Amanda Palmer, Jamie Austin, Wolf Schlager, and the rest of the scientists, technicians, officers, and crew aboard the *JOIDES Resolution* for their help and support. A particularly thoughtful review by Fritz Theyer greatly improved the manuscript.

REFERENCES

Andrews, J. A., 1985. True polar wander: an analysis of Cenozoic and Mesozoic paleomagnetic poles. *J. Geophys. Res.*, 90:7737–7750.

Austin, J. A., Schlager, W., et al., 1986. *Proc. ODP, Init. Repts.*, 101: College Station, TX (Ocean Drilling Program).

Berggren, W. A., Kent, D. V., Flynn, J. J., and Van Couvering, J. A., 1985. Cenozoic geochronology. *Geol. Soc. Am. Bull.*, 96:1407–1418.

Champion, D. E., Dalrymple, G. B., and Kuntz, M. A., 1981. Radiometric and paleomagnetic evidence for the Emperor reversed polarity event at 0.46 ± 0.05 m.y. in basalt lava flows from the eastern Snake River Plain, Idaho. *Geophys. Res. Lett.*, 8:1055–1058.

Chave, A., 1984. Lower Paleocene–Upper Cretaceous magnetostratigraphy, Sites 525, 527, 528, and 529, Deep Sea Drilling Project Leg 74. *In* Moore, T. C., Jr., Rabinowitz, P. D., et al., *Init. Repts. DSDP*, 74: Washington (U.S. Govt. Printing Office), 525–531.

Clement, B. M., and Kent, D. V., 1987. Short polarity intervals within the Matuyama: transitional field records from hydraulic piston cored sediments from the North Atlantic. *Earth Planet. Sci. Lett.*, 81:253–264.

Coe, R. S., Gromme, S., and Mankinen, E. A., 1978. Geomagnetic paleointensities from radiocarbon-dated lava flows on Hawaii and the question of the Pacific nondipole low. *J. Geophys. Res.*, 83:1740–1756.

Coupland, D. H., and Van der Voo, R., 1980. Long-term nondipole components in the geomagnetic field during the last 130 m.y. *J. Geophys. Res.*, 85:3529–3548.

Cox, A., and Gordon, R. G., 1984. Paleolatitudes determined from paleomagnetic data from vertical cores. *Rev. Geophys. Space Phys.*, 22:47–72.

Epp, D., Sager, W. W., Theyer, F., and Hammond, S. R., 1983. Hot-spot-spin axis motion or magnetic far-sided effect? *Nature*, 303: 318–320.

Fisher, R. A., 1953. Dispersion on a sphere. *Proc. R. Soc. London*, A217:295–305.

Gordon, R. G., Cox, A., and O'Hare, S., 1984. Paleomagnetic Euler poles and the apparent polar wander and absolute motion of North America since the Carboniferous. *Tectonics*, 3:499–537.

Harland, W. B., Cox, A. V., Llewellyn, P. G., Pickton, C.A.G., Smith, A. G., and Walters, R., 1982. *A Geologic Time Scale.* Cambridge (Cambridge Univ. Press).

Harrison, C.G.A., and Lindh, T., 1982. A polar wandering curve for North America during the Mesozoic and Cenozoic. *J. Geophys. Res.*, 87:1903–1920.

Heath, G. R., Rea, D. H., and Levi, S., 1985. Paleomagnetism and accumulation rates of sediments at Sites 576 and 578, Deep Sea Drilling Project Leg 86, Western North Pacific. *In* Heath, G. R., Burckle, L. H., et al., *Init. Repts. DSDP*, 86: Washington (U.S. Govt. Printing Office), 459–502.

Jurdy, D. M., 1981. True polar wander. *Tectonophysics*, 74:1–16.

Karlin, R., 1987. Effects of sampling technique on paleomagnetic directions in wet sediments. *Eos, Am. Geophys. Union Trans.*, 68:298. (Abstract)

Karlin, R., and Levi, S., 1983. Diagenesis of magnetic minerals in recent haemipelagic sediments. *Nature*, 303:327–330.

_____, 1985. Geochemical and sedimentological control of the magnetic properties of hemipelagic sediments. *J. Geophys. Res.*, 90: 10373–10392.

Karlin, R., Lyle, M., and Heath, G. R., 1987. Authigenic magnetite formation in suboxic marine sediments. *Nature*, 326:490–492.

Kent, D. V., and Gradstein, F. M., 1985. A Cretaceous and Jurassic geochronology. *Geol. Soc. Am. Bull.*, 96:1419–1427.

Kent, D. V., and Spariosu, D. J., 1982a. Magnetostratigraphy of Caribbean Site 502 hydraulic piston cores. *In* Prell, W. L., Gardner, J. V., et al., *Init. Repts. DSDP*, 68: Washington (U.S. Govt. Printing Office), 419–433.

_____, 1982b. Magnetostratigraphy of equatorial Pacific Site 503 hydraulic piston cores. *In* Prell, W. L., Gardner, J. V., et al. *Init. Repts. DSDP*, 68: Washington (U.S. Govt. Printing Office), 435–440.

Kirshvink, J. L., 1982. Paleomagnetic evidence for fossil biogenic magnetite in western Crete. *Earth Planet. Sci. Lett.*, 59:388–392.

Kirshvink, J. L., and Chang, S.-B. R., 1984. Ultrafine-grained magnetite in deep-sea sediments: possible bacterial magnetofossils. *Geology*, 12:559–562.

Kirshvink, J. L., and Lowenstam, H. A., 1979. Mineralization and magnetization of chiton teeth: paleomagnetic, sedimentologic, and biologic implications of organic magnetite. *Earth Planet. Sci. Lett.*, 44: 193–204.

Klitgord, K. D., and Schouten, H., 1986. Plate kinematics of the central Atlantic. *In* Vogt, P. R., and Tucholke, B. E., *The Geology of North America*, vol. M: Geol. Soc. Am., 351–378.

Kono, M., 1980. Statistics of paleomagnetic inclination data. *J. Geophys. Res.*, 85:3878–3882.

Leslie, B., Hammond, D. E., Lund, S., and Hamilton, M., 1984. Diagenesis of iron and sulphur in sediments of the CCB. *Eos, Am. Geophys. Union Trans.*, 65:958. (Abstract)

Livermore, R. A., Vine, F. J., and Smith, A. G., 1983. Plate motions and the geomagnetic field—I. Quaternary and Late Tertiary. *Geophys. J. R. Astron. Soc.*, 73:153–171.

_____, 1984. Plate motions and the geomagnetic field—II. Jurassic to Tertiary. *Geophys. J. R. Astron. Soc.*, 79:939–961.

McDougall, I., 1979. The present status of the geomagnetic polarity timescale. *In* McElhinny, M. W. (Ed.), *The Earth: Its Origin, Evolution and Structure*: London (Academic Press), 543–566.

McFadden, P. L., and Reid, A. B., 1982. Analysis of palaeomagnetic inclination data. *Geophys. J. R. Astron. Soc.*, 69:307–319.

McNeil, D. F., Ginsburg, R. N., Chang, S-B. R., and Kirschvink, J. L., 1987. A biogenic magnetic source in Plio-Pleistocene shallow-water carbonate rocks, Bahamas. *Eos, Am. Geophys. Union Trans.*, 68: 297. (Abstract)

Merrill, R. T., and McElhinny, M. W., 1977. Anomalies in the time-averaged paleomagnetic field and their implications for the lower mantle. *Rev. Geophys. Space Phys.*, 15:309–323.

Morgan, W. J., 1983. Hotspot tracks and the early rifting of the Atlantic. *Tectonophysics*, 94:123–139.

Ogg, J. G., 1983. Magnetostratigraphy of Upper Jurassic and lowest Cretaceous sediments, Deep Sea Drilling Project Site 534, western North Atlantic. *In* Sheridan, R. E., Gradstein, F. M., et al., *Init. Repts. DSDP*, 76: Washington (U.S. Govt. Printing Office), 685–697.

_____, 1985. Paleolatitudes and magnetostratigraphy of Cretaceous and lower Tertiary rocks, Deep Sea Drilling Project Site 585, Mariana Basin, Western Central Pacific. *In* Moberly, R. Schlanger, S. O., et al., *Init. Repts. DSDP*, 89: Washington (U.S. Govt. Printing Office), 629–645.

Ogg, J. G., and Lowrie, W., 1986. Magnetostratigraphy of the Jurassic/Cretaceous boundary. *Geology*, 14:547–550.

Petersen, N., von Dobeneck, T., and Vali, H., 1986. Fossil bacterial magnetite in deep-sea sediments from the South Atlantic Ocean. *Nature*, 320:611–615.

Reynolds, R. L., Karachewski, J. A., Fishman, N. S., and Rosenbaum, J. G., 1986. Magnetic properties of greigite-bearing Cretaceous strata, North Slope Alaska. *Eos, Am. Geophys. Union Trans.*, 67:923. (Abstract)

Sager, W. W., 1984. Paleomagnetism of Abbott Seamount and implications for the latitudinal drift of the Hawaiian hot spot. *J. Geophys. Res.*, 89:6271–6284.

Stoltz, J. F., Chang, S-B. R., and Kirshvink, J. L., 1986. Magnetotactic bacteria and single-domain magnetite in hemipelagic sediments. *Nature*, 321:849–850.

Tarling, D. H., 1983. *Palaeomagnetism*: London (Chapman and Hall).

Tauxe, L., Tucker, P., Petersen, N., and LaBrecque, J. L., 1984. Magnetostratigraphy of Leg 73 sediments. *In* Hsü, K. J., LaBrecque, J. L., et al., *Init. Repts. DSDP*, 73: Washington (U.S. Govt. Printing Office), 609–622.

Verosub, K. L., and Banerjee, S. K., 1977. Geomagnetic excursions and their paleomagnetic record. *Rev. Geophys. Space Phys.*, 15:145–155.

Weinreich, N., and Theyer, F., 1985. Paleomagnetism of Deep Sea Drilling Project Leg 85 sediments: Neogene magnetostratigraphy and tectonic history of the central equatorial Pacific. *In* Mayer, L., Theyer, F., et al., *Init. Repts. DSDP*, 85: Washington (U.S. Govt. Printing Office), 849–901.

Wilson, R. L., 1971. Dipole offset—the time-averaged palaeomagnetic field over the past 25 million years. *Geophys. J. R. Astron. Soc.*, 22: 491–504.

Date of initial receipt: 2 March 1987
Date of acceptance: 24 September 1987
Ms 101B-153

APPENDIX
Paleomagnetic Measurements

SAMPLE #	DEPTH (cm)	STEP	INCLI. (Down)	DECLI. (East)	NRM Jo (mA/m)	J/Jo	CSD	MDF (mT)
HOLE 626B								
5-1-059	14789	AF700	-36.7	91.9	0.23E-06	0.00	23.05	
5-2-090	14970	AF100	-26.0	61.5	0.27E+02	0.62	6.70	
HOLE 626C								
4-1-087	2637	NRM	*	*	0.19E+02	*	*	
4-1-093	2643	AF100	-18.2	340.8	0.19E+02	0.48	0.37	
4-1-100	2650	NRM	*	*	0.26E+02	*	*	
4-2-025	2725	AF100	-23.4	14.0	0.90E+02	0.62	0.09	
4-2-070	2770	NRM	*	*	0.22E+02	*	*	
14-1-010	12180	AF100	-6.7	177.1	0.50E-01	0.79	2.25	
14-2-014	12334	AF100	44.0	99.9	0.84E-01	0.63	1.20	
14-2-128	12448	AF100	32.1	148.5	0.24E-01	0.70	3.59	
14-3-090	12560	AF100	-4.6	359.3	0.20E-01	0.88	4.27	
14-3-151	12621	NRM	*	*	0.37E+00	*	*	
14-4-015	12635	AF100	-67.3	228.8	0.23E+00	0.90	0.97	
14-4-110	12730	AF100	50.0	276.3	0.22E-01	0.89	4.41	
14-5-015	12785	AF100	12.0	137.6	0.14E-01	0.69	16.28	
14-6-015	12935	AF100	-2.5	132.8	0.20E-01	0.77	2.78	
15-1-015	13145	AF100	79.1	3.9	0.44E-01	0.66	4.16	
15-2-015	13295	NRM	*	*	0.15E-01	*	*	
15-3-015	13445	AF100	-54.6	237.4	0.36E-02	1.25	9.88	
15-4-015	13595	AF100	-27.9	203.0	0.42E-01	0.80	1.77	
15-5-015	13745	AF100	-63.9	115.7	0.12E-01	0.86	6.44	
15-6-015	13895	AF100	16.4	277.0	0.11E-01	0.55	5.09	
15-7-015	14045	AF100	-76.9	9.8	0.61E-01	0.90	1.25	
16-1-029	14109	AF100	-57.0	165.4	0.80E-02	0.93	16.14	
16-2-022	14252	AF100	-17.3	223.9	0.23E+00	0.96	0.43	
16-3-030	14410	AF100	-47.9	48.8	0.20E-01	1.24	2.90	
16-4-038	14568	AF100	-18.2	275.0	0.17E-01	1.25	9.55	
16-5-010	14690	AF100	2.6	158.8	0.73E-01	0.79	1.87	
16-6-030	14860	AF100	1.2	207.3	0.32E-01	1.09	2.46	
18-1-073	16073	NRM	*	*	0.29E-01	*	*	
18-2-043	16193	AF100	49.6	24.5	0.73E-01	0.83	1.65	
18-3-068	16368	AF100	72.0	294.2	0.11E-01	0.48	7.77	
18-4-055	16505	AF100	12.4	277.1	0.49E-02	1.62	10.71	
18-5-055	16655	AF100	19.0	172.0	0.25E-01	0.91	4.51	
18-6-130	16880	AF100	85.1	127.6	0.21E-01	0.84	2.02	
HOLE 627B								
1-2-020	170	AF500	30.1	21.2	0.21E+01	0.47	0.64	48.8
1-3-070	370	AF500	36.0	344.1	0.22E+01	0.18	3.22	25.6
1-3-123	423	AF600	2.8	10.3	0.76E+00	0.95	0.69	
1-4-060	510	AF600	30.1	69.5	0.27E-01	0.48	3.35	57.1
2-2-090	820	AF300	32.2	55.7	0.55E-01	0.48	3.43	26.7
2-3-050	930	AF300	-68.5	168.3	0.26E-01	0.76	3.04	35.3
2-3-100	980	AF200	5.3	57.5	0.12E+00	0.14	1.83	6.9
2-4-031	1061	AF200	-25.0	345.0	0.16E-01	0.68	2.94	20.9
2-4-068	1098	NRM	*	*	0.38E+00	*	*	
2-4-080	1110	AF100	-77.4	11.2	0.16E+00	0.21	1.58	6.3
2-4-090	1120	AF400	-51.7	156.9	0.30E-01	0.57	3.07	42.8
2-5-031	1211	AF600	19.7	74.8	0.28E-01	0.58	2.66	66.5
2-5-062	1242	AF300	-34.1	297.6	0.16E+00	0.38	0.55	23.3
2-5-110	1290	AF300	-28.0	13.7	0.57E-01	0.36	4.97	25.1

Abbreviations:

STEP Maximum step of demagnetization (AF) alternating field or (TH) thermal, at which characteristic remanence direction was measured
INCLI. Inclination of characteristic remanence
DECLI. Declination of characteristic remanence

SAMPLE #	DEPTH (cm)	STEP	INCLI. (Down)	DECLI. (East)	NRM Jo (mA/m)	J/Jo	CSD	MDF (mT)
2-6-030	1360	AF100	-26.4	22.0	0.43E-01	0.81	4.38	23.4
2-6-090	1420	AF100	35.0	40.5	0.96E-01	0.21	2.35	6.2
2-6-106	1436	AF300	-6.1	65.7	0.43E-01	0.56	3.17	
3-1-036	1586	AF100	38.1	64.8	0.11E+00	0.72	1.28	
3-1-088	1638	AF400	23.9	52.9	0.64E-01	0.46	3.65	28.5
3-2-033	1733	AF500	13.5	100.0	0.53E-01	0.49	3.23	47.5
3-2-104	1804	AF200	58.5	168.8	0.11E+00	0.29	2.82	8.2
3-3-116	1966	AF500	35.9	82.9	0.71E-01	0.38	1.96	43.5
3-3-128	1978	AF200	43.0	91.7	0.98E-01	0.41	1.52	12.1
3-4-062	2062	AF300	-14.6	102.2	0.63E-01	0.34	2.99	24.9
3-4-133	2133	AF300	41.7	73.0	0.53E-01	0.68	2.54	48.1
3-5-018	2168	AF200	11.3	152.1	0.38E-01	0.31	10.76	16.2
3-5-096	2246	AF400	43.0	75.8	0.13E+00	0.41	1.11	33.8
3-6-055	2355	AF300	49.2	126.3	0.91E-01	0.69	0.67	49.3
3-6-118	2418	AF300	22.3	118.2	0.93E-01	0.37	2.86	20.7
3-7-039	2489	AF300	55.8	92.2	0.14E+00	0.41	0.82	21.5
4-1-045	2565	AF400	42.1	54.3	0.17E+00	0.32	0.96	25.3
4-1-130	2650	AF100	38.0	26.5	0.29E+00	0.47	0.76	9.3
4-2-045	2715	AF100	25.2	45.4	0.86E-01	0.25	4.29	5.5
4-2-126	2796	AF100	9.4	333.9	0.74E-01	0.71	1.40	
4-3-069	2889	AF200	-41.2	350.2	0.15E+00	0.60	1.81	23.7
4-3-112	2932	AF400	5.2	64.2	0.17E+00	0.64	0.86	47.1
4-4-015	2985	AF100	-58.6	109.8	0.55E-01	1.17	2.67	
4-4-084	3054	AF100	-28.3	92.3	0.61E-01	0.28	3.66	6.0
4-5-026	3146	AF100	32.9	156.0	0.20E-01	0.35	19.37	
4-5-070	3190	AF125	54.4	174.3	0.71E-01	0.49	2.10	11.9
4-6-110	3380	AF100	47.5	57.9	0.13E+00	0.56	1.74	
4-6-140	3410	AF300	45.0	95.1	0.92E-01	0.44	0.93	24.6
4-7-010	3430	AF100	74.6	38.1	0.10E+00	0.71	0.93	
5-1-060	3530	AF100	70.1	158.6	0.17E-01	0.70	4.09	
5-2-036	3656	AF100	23.1	119.0	0.30E-01	0.41	7.68	7.5
5-2-100	3720	AF200	26.9	106.2	0.69E-01	0.65	2.46	
5-3-088	3858	AF100	27.5	88.3	0.19E-01	0.51	4.06	
5-3-140	3910	AF200	-37.9	221.3	0.42E-01	0.33	2.98	14.1
5-4-090	4010	AF100	-63.4	213.0	0.15E-01	0.29	12.36	7.7
5-5-090	4160	AF100	49.5	79.2	0.39E-01	0.35	6.98	8.3
5-6-090	4310	AF200	50.8	74.0	0.51E-01	0.38	7.37	16.9
6-1-060	4480	AF100	36.6	115.9	0.14E-01	0.39	6.62	8.5
6-1-117	4537	AF100	-13.0	252.4	0.46E-02	1.81	5.36	
6-2-090	4660	AF50	-44.9	275.1	0.11E-01	0.90	5.22	
6-3-090	4810	AF100	3.4	327.5	0.12E-01	0.63	7.87	
6-4-013	4883	AF100	18.0	290.5	0.22E-01	0.72	3.15	
6-4-089	4959	AF100	-68.4	26.6	0.87E-02	1.12	4.04	
6-5-013	5033	AF100	16.7	242.1	0.10E-01	1.35	3.29	
6-5-090	5110	AF100	-12.7	341.4	0.16E-01	0.51	3.33	9.4
6-6-090	5260	AF100	-46.2	83.0	0.84E-02	0.71	5.45	9.7
7-1-142	5522	AF100	68.3	143.0	0.30E-01	0.87	1.48	
7-2-090	5620	AF100	-18.1	285.3	0.13E-01	0.49	6.53	8.2
7-3-030	5710	AF100	-43.2	335.9	0.15E-01	2.28	5.74	
7-3-085	5765	AF100	-38.1	321.3	0.23E-01	2.26	1.56	
7-3-136	5816	AF500	-63.0	322.0	0.65E-01	0.34	2.24	42.0
7-4-045	5875	AF200	45.6	136.0	0.52E-01	0.55	5.11	17.2
7-4-102	5932	AF100	74.2	251.0	0.37E-01	0.51	4.27	8.3
7-5-105	6085	AF50	-18.3	70.2	0.68E-02	1.32	8.45	
7-6-110	6240	AF050	-17.1	75.9	0.98E-02	0.49	10.26	6.4

* Indicates no stable characteristic remanence found
NRM Jo Intensity of NRM in milliamps per meter
J/Jo Intensity of characteristic magnetization (at given step) divided by NRM intensity
CSD Circular standard deviation of characteristic remanence vector
MDF Mean destructive field, in milliTeslas

SAMPLE #	DEPTH (cm)	STEP	INCLI. (Down)	DECLI. (East)	NRM Jo (mA/m)	J/Jo	CSD	MDF (mT)
8-1-068	6398	AF100	-11.0	8.7	0.88E-02	0.50	10.82	8.9
8-2-068	6548	AF200	-76.9	257.3	0.72E+00	0.69	0.51	
8-3-068	6698	AF100	88.2	147.5	0.33E-01	0.71	2.47	
8-4-095	6875	AF100	-0.8	1.8	0.21E-01	0.36	8.01	7.1
8-5-054	6984	AF100	67.5	54.5	0.49E-01	0.28	8.56	6.5
8-5-084	7014	AF100	69.4	303.5	0.29E-01	0.79	3.17	
8-5-140	7070	AF100	27.5	43.7	0.18E-01	0.21	9.99	4.0
8-6-020	7100	AF100	50.8	350.8	0.25E-01	0.45	7.57	8.8
8-6-084	7164	AF100	55.0	290.0	0.23E-01	0.50	4.17	10.0
9-2-100	7540	AF100	9.0	357.8	0.21E-01	0.33	11.35	
9-3-014	7604	AF100	-61.9	52.4	0.92E-02	1.15	3.90	
9-3-034	7624	AF100	4.9	295.4	0.15E+00	0.82	1.12	
9-3-084	7674	AF050	56.7	327.1	0.13E+00	0.62	3.14	8.8
9-3-110	7700	AF200	42.4	356.1	0.96E-01	0.50	1.69	18.9
9-4-100	7840	AF200	14.9	9.5	0.22E+00	0.48	1.97	18.5
9-5-090	7980	AF125	34.9	168.5	0.86E-01	0.28	1.28	6.9
9-6-090	8130	AF200	39.1	73.7	0.16E+00	0.55	1.82	17.9
10-1-110	8360	AF50	-66.2	177.9	0.11E-01	0.72	5.60	
10-2-110	8510	AF200	52.8	165.0	0.94E-01	0.44	1.24	17.5
10-3-120	8670	AF200	-47.8	62.2	0.62E-01	0.06	11.09	10.5
10-4-090	8790	AF125	58.6	255.7	0.63E-01	0.33	2.41	8.2
10-5-045	8895	AF100	14.3	288.8	0.17E-01	1.16	3.47	
10-5-090	8940	AF50	26.1	336.0	0.14E-01	0.85	5.03	
10-6-084	9084	AF100	51.1	4.0	0.37E-01	0.51	8.65	8.9
10-6-130	9130	AF50	19.0	73.1	0.35E-02	2.79	5.07	
10-7-025	9175	AF100	38.0	350.9	0.11E-01	0.44	13.60	
11-1-030	9230	AF300	78.9	233.7	0.13E+00	0.11	4.19	15.7
11-1-054	9254	AF100	30.9	30.1	0.88E-01	0.45	1.45	8.8
11-1-110	9310	AF50	-32.1	44.5	0.83E-02	1.06	11.74	
11-2-110	9460	AF100	-36.5	24.2	0.21E-01	0.76	5.14	
11-3-054	9554	AF100	35.6	337.9	0.30E-01	0.38	13.67	
11-3-130	9630	AF125	45.2	74.3	0.29E-01	0.39	6.37	8.8
11-4-030	9680	AF100	19.0	355.3	0.18E-01	0.44	10.86	9.3
11-4-130	9780	AF50	17.4	28.1	0.75E-02	0.59	5.18	4.6
11-5-088	9888	AF50	-3.2	327.7	0.35E-02	1.32	9.87	
11-6-110	10060	AF50	40.3	27.3	0.12E-01	1.26	4.39	
12-1-070	10220	AF100	65.0	51.3	0.33E-01	0.22	29.93	6.6
12-1-134	10284	AF100	34.5	188.7	0.32E-01	0.89	2.95	
12-2-086	10386	AF100	21.6	116.7	0.19E-01	0.31	6.05	7.1
12-2-134	10434	AF100	-65.6	52.8	0.13E-01	0.76	5.34	
12-3-134	10584	AF100	11.9	267.6	0.31E-01	0.74	3.25	
12-4-124	10724	AF100	-8.7	271.7	0.43E-01	0.89	1.20	
12-5-045	10795	AF50	51.5	69.7	0.90E-02	1.64	4.62	
12-5-086	10836	AF100	79.9	102.2	0.65E-01	2.19	0.72	
12-6-034	10934	AF100	13.5	232.1	0.29E-01	0.33	6.65	8.2
12-6-120	11020	AF100	84.4	135.1	0.14E-01	0.61	7.63	
12-7-042	11092	AF100	-0.4	265.5	0.10E+00	1.13	0.89	
13-2-060	11340	AF50	29.4	25.5	0.82E-02	1.48	6.81	
13-3-014	11444	AF100	73.5	36.6	0.38E-01	0.77	1.88	
13-3-045	11475	NRM	*	*	0.47E-01	*	*	
13-3-090	11520	AF50	-6.0	8.3	0.48E-02	1.84	7.56	
13-4-032	11612	AF050	-2.5	55.3	0.14E-01	0.28	8.61	3.2
13-5-090	11820	AF050	65.3	145.7	0.58E-02	1.31	5.00	
13-6-014	11894	AF100	-19.6	15.2	0.16E-01	0.32	28.17	8.3
13-6-045	11925	AF100	69.1	141.1	0.11E-01	0.52	13.52	9.8

Abbreviations:

STEP Maximum step of demagnetization, (AF) alternating field or (TH) thermal, at which characteristic remanence direction was measured
INCLI. Inclination of characteristic remanence
DECLI. Declination of characteristic remanence
* Indicates no stable characteristic remanence found

SAMPLE #	DEPTH (cm)	STEP	INCLI. (Down)	DECLI. (East)	NRM Jo (mA/m)	J/Jo	CSD	MDF (mT)
13-7-014	12044	AF100	-85.4	348.8	0.70E-01	1.00	0.94	
14-1-035	12115	AF050	12.5	348.8	0.13E-01	0.82	4.31	
14-1-095	12175	AF100	42.4	83.7	0.58E-01	0.49	4.15	9.6
14-2-035	12265	AF050	14.5	216.5	0.12E-01	0.92	2.38	
14-2-134	12364	NRM	*	*	0.22E-02	*	*	
14-3-035	12415	AF050	-38.4	117.6	0.67E-02	0.57	8.11	
14-3-096	12476	AF100	23.5	162.0	0.17E-01	0.73	5.02	
14-4-013	12543	AF100	-39.1	245.6	0.11E+00	1.03	1.33	
14-4-110	12640	AF200	-21.5	64.4	0.44E-01	0.61	3.81	28.8
14-5-013	12693	AF300	23.3	36.9	0.22E+00	0.31	1.45	22.6
14-6-045	12875	AF050	56.2	214.5	0.22E-01	0.74	1.78	
14-6-126	12956	AF100	54.2	305.1	0.91E-01	0.47	1.48	8.6
14-7-014	12994	AF100	47.4	348.3	0.23E-01	0.45	6.29	9.1
15-1-070	13100	AF050	27.3	215.1	0.14E-01	0.85	2.51	
15-1-143	13173	AF100	41.2	160.8	0.62E-01	0.44	2.82	8.5
15-2-024	13204	AF100	78.8	87.3	0.13E+00	0.55	0.98	
15-2-100	13280	AF100	60.8	140.5	0.58E-01	0.45	1.38	8.8
15-3-070	13400	AF050	54.7	136.1	0.23E-01	1.02	3.26	
15-3-143	13473	AF100	4.0	242.1	0.22E-01	0.74	2.51	
15-4-024	13504	NRM	*	*	0.43E-01	*	*	
15-4-065	13545	AF100	63.6	241.4	0.38E-01	0.37	3.49	7.2
15-4-105	13585	AF300	-10.9	14.9	0.17E-01	0.58	6.73	11.6
15-5-020	13650	AF050	40.3	137.8	0.45E-02	1.03	4.69	
16-1-045	14035	AF100	52.6	32.4	0.38E-01	0.22	3.53	6.4
16-1-120	14110	AF050	-20.0	93.5	0.12E-01	0.68	8.14	
16-2-045	14185	AF100	68.8	91.8	0.29E-01	0.61	2.34	
16-2-130	14270	AF050	6.2	288.3	0.56E-02	1.60	4.48	
16-3-045	14335	AF100	34.9	52.9	0.12E+00	0.41	2.32	6.8
16-3-125	14415	AF050	-46.6	217.0	0.20E-01	1.09	2.60	
16-4-130	14570	AF150	47.2	53.4	0.38E-01	0.50	4.04	15.0
16-5-045	14635	TH250	40.7	62.7	0.97E-01	0.52	2.49	
16-5-110	14700	AF100	-28.6	85.2	0.27E-01	0.68	1.30	
16-6-115	14855	AF100	-49.4	49.9	0.54E-01	0.85	1.04	
17-2-038	15158	AF100	28.4	356.1	0.16E-01	0.30	13.95	7.8
17-2-054	15174	AF100	28.1	270.5	0.24E+01	0.92	0.18	
17-3-054	15324	AF600	45.4	13.3	0.48E+01	0.61	0.69	85.0
17-4-038	15458	AF100	6.6	60.0	0.45E-01	0.34	3.10	
17-4-054	15474	AF100	-21.0	166.7	0.23E-01	0.48	4.53	8.9
18-2-035	16405	AF100	-3.4	195.3	0.13E-01	0.23	13.82	5.6
20-1-070	18210	AF100	-8.2	48.7	0.37E-01	1.17	1.40	
26-1-054	23964	AF400	41.9	289.7	0.16E+01	0.25	0.36	
26-1-067	23977	AF400	73.2	130.9	0.15E+01	0.18	0.56	
26-1-092	24002	AF400	32.8	329.4	0.11E+01	0.36	1.31	23.3
26-1-114	24024	AF400	62.4	252.4	0.33E+00	0.54	0.49	
26-1-126	24036	AF400	5.8	304.8	0.79E+00	0.10	0.55	
26-1-140	24050	AF400	-3.3	302.6	0.25E+00	0.18	2.45	
26-2-012	24072	AF400	30.3	314.9	0.94E+00	0.21	0.79	
26-0-014	24126	TH250	35.5	57.3	0.22E+01	0.33	1.70	
27-1-044	24914	AF400	-2.3	29.2	0.14E+01	0.18	0.23	
27-1-056	24926	AF800	10.9	248.4	0.15E+01	0.18	7.75	37.6
27-1-073	24943	AF400	76.1	197.2	0.15E+01	0.04	0.36	
27-1-138	25008	AF400	51.0	159.4	0.11E+01	0.57	0.25	
27-2-075	25095	AF500	37.1	238.9	0.65E+00	0.40	24.28	40.8
27-2-111	25131	AF400	78.8	224.0	0.11E+01	0.22	3.42	27.5
27-4-025	25345	AF400	23.7	124.6	0.53E+00	0.50	0.88	

NRM Jo Intensity of NRM in milliamps per meter
J/Jo Intensity of characteristic magnetization (at given step) divided by NRM intensity
CSD Circular standard deviation of characteristic remanence vector
MDF Mean destructive field, in milliTeslas

SAMPLE #	DEPTH (cm)	STEP	INCLI. (Down)	DECLI. (East)	NRM Jo (mA/m)	J/Jo	CSD	MDF (mT)
27-4-070	25390	AF400	39.1	123.1	0.12E+01	0.19	0.50	
27-4-130	25450	AF400	65.8	208.0	0.52E+00	0.23	0.58	
27-4-139	25459	AF400	33.2	335.8	0.13E+01	0.11	0.84	
27-6-063	25683	AF400	61.2	291.3	0.16E+01	0.35	1.60	21.2
27-6-125	25745	AF600	80.3	194.8	0.14E+01	0.28	2.78	35.7
28-1-113	25933	AF400	0.0	309.9	0.28E+01	0.57	0.27	
28-1-116	25936	AF400	6.3	289.7	0.23E+01	0.34	0.39	
28-1-136	25956	AF400	-20.2	296.1	0.28E+01	0.47	0.46	
28-2-010	25980	AF600	-15.6	303.7	0.16E+01	0.30	2.75	50.5
28-2-113	26083	AF600	39.6	343.0	0.29E+01	0.19	2.71	29.4
28-4-017	26287	AF400	-6.1	126.1	0.22E+01	0.55	0.39	
28-4-020	26290	AF400	-10.4	113.5	0.30E+01	0.37	0.31	
28-4-107	26377	AF500	-36.9	288.1	0.90E+00	0.63	4.68	58.7
28-4-134	26404	AF400	-19.7	243.4	0.10E+01	0.45	0.55	
28-5-098	26518	AF400	45.8	4.2	0.23E+01	0.33	1.55	24.5
28-6-024	26594	AF400	48.5	86.6	0.24E+01	0.24	2.85	16.7
29-2-038	26938	NRM	*	*	0.54E+00	*	*	
29-2-062	26962	NRM	*	*	0.96E+00	*	*	
29-2-064	26964	TH500	31.7	247.4	0.41E+00	0.97	0.94	
29-2-134	27034	TH550	27.4	123.5	0.18E+01	0.33	5.09	
29-2-138	27038	TH550	23.2	115.2	0.18E+01	0.41	1.04	
29-4-016	27216	AF600	58.2	177.9	0.14E+01	0.42	5.76	16.7
29-4-108	27308	AF500	45.3	38.9	0.12E+01	0.43	3.74	45.9
29-5-055	27405	TH300	29.4	210.9	0.50E+01	0.34	1.14	
29-5-058	27408	TH300	29.9	209.2	0.46E+01	0.46	2.11	
29-5-067	27417	TH300	29.9	197.0	0.22E+01	0.57	0.73	
29-5-072	27422	TH300	27.0	190.4	0.58E+01	0.35	1.57	
29-5-107	27457	AF400	43.9	132.3	0.19E+01	0.32	0.31	
29-6-124	27624	AF400	46.7	329.2	0.67E+01	0.30	1.08	23.3
30-1-079	27739	AF400	41.3	62.4	0.18E+01	0.36	3.99	28.3
30-3-036	27996	AF300	28.6	58.1	0.37E+01	0.35	2.76	16.1
30-3-128	28088	AF200	27.0	70.9	0.22E+01	0.77	0.03	
31-2-087	28867	AF400	15.5	346.0	0.27E+01	0.47	1.92	37.5
31-3-074	29004	TH300	42.0	324.5	0.52E+01	0.31	1.40	
31-3-079	29009	AF400	60.2	249.3	0.39E+01	0.19	0.21	
31-4-012	29092	AF200	65.2	89.8	0.14E+00	0.61	0.58	
31-4-098	29178	TH300	42.4	293.0	0.28E+00	0.49	0.72	
32-2-035	29785	AF400	38.1	235.6	0.12E+00	0.46	1.32	37.2
32-4-067	30117	AF200	34.1	56.0	0.84E-01	0.68	1.34	
32-4-143	30193	AF400	39.3	19.6	0.25E+00	0.34	1.12	22.9
32-6-007	30357	AF200	42.4	353.6	0.24E+00	0.58	0.82	
32-6-111	30461	AF400	67.5	184.3	0.37E+00	0.43	1.06	35.8
33-1-065	30625	AF200	-34.4	336.7	0.58E+00	0.94	0.17	
33-2-093	30803	AF200	47.9	87.7	0.19E+00	0.52	0.46	
33-0-040	30854	TH300	42.9	277.6	0.78E+01	0.00	0.78	
34-1-083	31583	TH300	47.1	174.5	0.17E+00	0.72	1.17	
34-1-141	31641	TH450	38.5	191.1	0.20E+00	0.18	2.61	
34-4-134	32084	AF400	29.1	342.2	0.21E+00	0.30	2.54	29.2
34-5-104	32204	TH300	43.8	308.5	0.45E+00	0.41	0.64	
34-6-016	32266	TH300	43.8	303.8	0.40E+00	0.45	1.01	
34-6-035	32285	AF200	52.5	260.4	0.26E+00	0.77	0.22	
34-6-078	32328	TH300	50.0	331.0	0.89E+00	0.41	1.20	
37-1-021	34411	TH300	21.7	58.8	0.21E-01	0.40	10.98	
37-1-033	34423	TH250	-59.3	300.9	0.28E-01	0.58	2.84	
37-1-046	34436	TH250	10.5	181.0	0.17E-01	0.96	2.36	

Abbreviations:

STEP Maximum step of demagnetization, (AF) alternating field or (TH) thermal, at which characteristic remanence direction was measured
INCLI. Inclination of characteristic remanence
DECLI. Declination of characteristic remanence

SAMPLE #	DEPTH (cm)	STEP	INCLI. (Down)	DECLI. (East)	NRM Jo (mA/m)	J/Jo	CSD	MDF (mT)
37-1-051	34441	TH250	20.8	168.6	0.23E-01	0.90	2.08	
37-1-056	34446	TH250	55.5	199.7	0.33E-01	0.42	2.41	
38-1-094	35444	TH250	35.6	165.4	0.20E+00	0.34	0.89	
38-1-134	35484	TH250	38.8	148.5	0.23E+00	0.38	0.30	
38-2-011	35511	TH250	33.7	137.6	0.25E+00	0.40	0.82	
38-2-108	35608	TH250	42.1	348.8	0.24E+00	0.42	0.71	
38-3-036	35686	TH250	63.5	220.9	0.28E+00	0.18	1.05	
38-3-095	35745	TH300	50.2	264.7	0.23E+00	0.16	1.51	
38-4-062	35862	TH300	49.4	344.9	0.20E+00	0.13	1.00	
38-4-129	35929	TH300	65.0	323.2	0.21E+00	0.16	1.40	
38-5-095	36045	TH300	60.3	325.9	0.25E+00	0.22	1.25	
38-5-122	36072	TH300	43.9	81.0	0.27E+00	0.15	4.31	
38-6-046	36146	TH300	46.1	23.1	0.23E+00	0.20	1.44	
38-0-025	36354	TH300	-65.8	160.4	0.19E+00	0.19	2.05	
39-1-059	36369	AF400	32.2	337.4	0.26E+00	0.44	0.68	
39-1-139	36449	AF400	44.2	150.6	0.16E+00	0.40	1.53	
39-2-017	36477	AF400	32.7	50.8	0.28E+00	0.49	1.04	
39-2-085	36545	TH300	62.5	4.0	0.17E+00	0.18	8.68	
39-2-112	36572	AF500	54.7	22.6	0.52E+00	0.18	0.87	17.5
39-2-125	36585	TH300	59.3	186.1	0.22E+00	0.43	1.44	
39-3-036	36646	TH300	67.5	355.7	0.17E+00	0.14	7.77	
39-3-068	36678	TH300	42.7	359.2	0.18E+00	0.23	2.11	
39-3-122	36732	TH300	40.8	6.2	0.16E+00	0.17	3.53	
39-4-092	36852	AF400	36.4	185.4	0.23E+00	0.42	0.89	
39-4-098	36858	TH200	35.4	170.7	0.15E+00	0.29	2.75	
39-4-123	36883	TH300	38.1	116.5	0.18E+00	0.08	5.21	
39-5-044	36954	TH300	72.7	275.3	0.14E+00	0.14	3.39	
39-5-109	37019	TH200	40.9	330.2	0.13E+00	0.22	3.62	
39-6-114	37174	TH200	44.2	68.9	0.18E+00	0.37	2.36	
39-0-006	37286	TH200	68.3	301.9	0.18E+00	0.29	1.26	
39-0-022	37302	TH200	26.5	213.1	0.21E+00	0.20	1.17	
40-1-055	37325	TH350	3.6	86.8	0.57E+00	0.45	1.38	
40-1-123	37393	TH250	77.6	254.2	0.14E+00	0.23	4.39	
40-2-018	37438	TH200	68.0	16.1	0.12E+00	0.27	1.44	
40-2-075	37495	TH200	59.6	62.9	0.12E+00	0.42	1.17	
40-3-113	37683	TH250	-29.6	273.6	0.17E+00	0.52	1.07	
40-4-023	37743	TH200	77.6	342.3	0.26E+00	0.50	1.26	
40-4-038	37758	TH200	37.5	203.3	0.19E+00	0.31	0.79	
40-4-138	37858	TH200	28.3	285.4	0.17E+00	0.36	0.83	
40-5-032	37902	TH200	65.5	106.5	0.16E+00	0.43	0.82	
40-6-056	38076	TH250	42.5	60.3	0.14E+00	0.15	1.39	
40-6-144	38164	TH200	55.7	134.9	0.13E+00	0.43	0.75	
41-1-060	38300	TH200	3.4	323.7	0.14E+00	0.29	1.11	
41-1-104	38344	TH200	44.4	284.4	0.18E+00	0.48	0.65	
41-2-022	38412	TH200	42.1	294.6	0.21E+00	0.57	0.34	
41-2-031	38421	TH250	53.3	279.8	0.22E+00	0.62	1.04	
41-2-088	38478	TH200	51.1	238.9	0.15E+00	0.51	0.27	
41-3-032	38572	TH200	66.7	53.5	0.15E+00	0.28	0.94	
41-3-109	38649	TH200	-10.1	102.9	0.23E+00	0.63	0.52	
41-4-028	38718	TH200	43.4	58.8	0.17E+00	0.53	0.88	
41-4-137	38827	TH200	55.8	130.3	0.30E+00	0.72	0.48	
41-5-026	38866	TH200	-53.3	40.1	0.10E+00	0.91	0.60	
41-5-147	38987	TH200	46.0	164.9	0.25E+00	0.41	0.44	
41-6-024	39014	TH200	60.7	197.5	0.15E+00	0.32	0.73	
41-6-136	39126	TH200	35.3	140.9	0.17E+00	0.38	0.50	

* Indicates no stable characteristic remanence found
NRM Jo Intensity of NRM in milliamps per meter
J/Jo Intensity of characteristic magnetization (at given step) divided by NRM intensity
CSD Circular standard deviation of characteristic remanence vector
MDF Mean destructive field, in milliTeslas

SAMPLE #	DEPTH (cm)	STEP	INCLI. (Down)	DECLI. (East)	NRM Jo (mA/m)	J/Jo	CSD	MDF (mT)
41-7-014	39154	TH400	-6.6	33.7	0.21E+00	0.20	3.99	
41-7-027	39167	TH200	65.7	297.9	0.15E+00	0.33	0.85	
42-1-066	39256	AF400	34.3	173.5	0.23E+00	0.50	0.50	
42-1-119	39309	AF400	27.2	60.3	0.21E+00	0.31	1.09	
42-2-042	39382	AF400	39.1	322.4	0.39E+00	0.17	2.12	4.9
42-2-131	39471	AF200	71.1	148.6	0.14E+00	0.44	0.82	
42-3-031	39521	AF200	-1.2	208.0	0.87E-01	0.52	1.73	
42-4-094	39734	AF200	38.6	233.2	0.18E+00	0.44	0.85	
42-5-032	39822	AF200	17.5	134.0	0.25E+00	0.52	1.11	
42-5-121	39911	AF200	57.8	40.7	0.27E+00	0.19	1.02	
42-6-061	40001	AF200	61.1	227.6	0.20E+00	0.46	0.51	
42-6-120	40060	AF200	52.3	16.9	0.13E+00	0.30	2.34	
43-1-002	40152	TH200	-49.7	225.2	0.18E+00	0.80	0.64	
43-1-089	40239	TH200	56.6	293.5	0.18E+00	0.70	0.35	
43-1-118	40268	TH300	49.3	214.9	0.18E+00	0.78	2.36	
43-2-033	40333	AF400	43.9	134.2	0.37E+00	0.13	1.38	9.2
43-2-117	40417	AF200	30.0	95.2	0.29E+00	0.44	0.37	
43-3-033	40483	AF200	44.4	3.4	0.32E+00	0.43	0.53	
43-3-124	40574	TH200	75.6	152.9	0.10E+00	0.61	0.89	
43-4-007	40607	AF200	-27.6	237.1	0.25E+01	0.02	0.36	
43-4-091	40691	TH200	17.5	354.6	0.85E-01	0.87	0.78	
43-5-021	40771	TH200	58.2	29.4	0.10E+00	0.58	0.71	
43-5-076	40826	TH200	47.4	74.6	0.15E+00	0.67	0.69	
43-6-035	40935	TH200	51.4	218.5	0.89E-01	0.69	0.75	
43-6-115	41015	TH200	53.4	249.3	0.12E+00	0.66	0.56	
43-7-025	41075	TH200	48.7	165.5	0.18E+00	0.62	0.54	
44-1-030	41140	TH200	38.3	181.3	0.13E+00	0.59	0.61	
44-1-089	41199	TH200	82.4	25.5	0.10E+00	0.59	0.86	
44-2-030	41290	TH200	45.3	239.3	0.17E+00	0.64	0.30	
44-2-089	41349	TH200	53.0	276.9	0.93E-01	0.54	0.45	
44-3-030	41440	TH200	47.7	95.3	0.11E+00	0.57	0.49	
44-3-091	41501	TH200	55.9	287.8	0.13E+00	0.60	0.40	
44-4-032	41592	AF600	43.6	343.7	0.19E+00	0.09	1.00	
44-4-089	41649	TH200	55.0	28.7	0.11E+00	0.78	0.42	
44-5-031	41741	TH200	33.4	256.9	0.16E+00	0.50	0.36	
44-5-091	41801	TH300	44.4	122.5	0.12E+00	0.54	2.45	
44-6-032	41892	TH200	51.1	338.5	0.84E-01	0.46	0.67	
44-6-085	41945	TH200	79.3	238.4	0.19E-01	0.77	1.30	
45-1-090	42160	TH200	42.8	7.8	0.77E-01	0.54	0.83	
46-1-047	43047	TH200	44.7	317.7	0.11E+00	0.57	0.70	
46-1-115	43115	AF200	58.9	88.8	0.11E+00	0.38	0.84	
46-2-036	43186	TH200	32.8	325.1	0.68E-01	0.38	0.65	
46-2-088	43238	AF200	45.2	48.4	0.13E+00	0.20	1.64	
46-3-010	43310	TH200	32.4	133.3	0.19E+00	0.39	0.49	
46-3-096	43396	AF200	44.6	342.9	0.13E+00	0.35	1.30	
46-4-071	43521	TH200	14.8	99.8	0.22E+00	0.89	0.20	
46-5-129	43729	TH300	56.0	60.1	0.18E+00	0.40	3.14	
46-6-055	43805	TH200	-69.6	20.8	0.53E-01	0.48	0.72	
46-6-139	43889	TH200	49.8	350.6	0.89E-01	0.48	0.69	
46-0-077	43970	TH200	32.8	232.6	0.10E+00	0.43	1.09	
47-1-025	43995	TH200	51.0	153.8	0.19E+00	0.39	0.63	
47-1-063	44033	TH200	49.3	44.0	0.32E+00	0.47	0.69	
47-2-014	44134	TH200	26.7	216.5	0.44E+00	0.69	0.18	
47-3-044	44314	TH200	27.3	146.5	0.16E+00	0.39	0.48	
47-3-134	44404	TH200	57.4	115.7	0.13E+00	0.38	0.78	

Abbreviations:

STEP Maximum step of demagnetization, (AF) alternating field or (TH) thermal, at which characteristic remanence direction was measured
INCLI. Inclination of characteristic remanence
DECLI. Declination of characteristic remanence

SAMPLE #	DEPTH (cm)	STEP	INCLI. (Down)	DECLI. (East)	NRM Jo (mA/m)	J/Jo	CSD	MDF (mT)
47-4-019	44439	TH200	37.1	265.5	0.12E+00	0.44	0.40	
47-4-108	44528	TH200	30.9	154.4	0.27E+00	0.28	0.74	
47-5-001	44571	TH200	54.4	143.7	0.28E+00	0.38	0.55	
47-5-085	44655	TH400	48.9	330.1	0.26E+00	0.09	2.34	
47-6-013	44733	TH200	65.4	190.4	0.17E+00	0.36	0.70	
47-6-082	44802	TH200	51.2	170.1	0.13E+00	0.48	0.21	
47-0-008	44941	TH200	43.2	10.5	0.74E-01	0.52	0.54	
HOLE 628A								
3-2-129	1599	AF100	-5.6	74.9	0.11E-01	0.99	6.18	
3-3-008	1628	AF100	-28.9	78.9	0.55E-02	1.95	2.80	
3-3-037	1657	AF100	-21.8	29.2	0.87E-02	1.07	3.53	
3-4-008	1778	AF100	49.5	103.3	0.33E-01	0.95	1.25	
3-6-120	2190	AF100	27.1	38.5	0.36E-01	0.81	0.96	
4-2-110	2550	AF300	51.5	226.5	0.77E-01	0.36	2.22	22.6
4-2-128	2568	AF100	51.6	281.7	0.46E-01	0.53	1.49	
4-3-128	2718	AF100	23.7	39.4	0.26E-01	0.47	3.10	
4-4-110	2850	AF100	4.6	30.2	0.14E-01	0.66	4.89	
4-6-110	3150	AF100	41.4	102.5	0.66E-01	0.75	1.02	
6-1-090	4280	AF100	-39.9	51.7	0.25E-01	0.95	1.84	
6-2-090	4430	AF100	27.6	57.2	0.22E-01	1.14	2.86	
6-3-090	4580	AF100	-23.3	91.0	0.93E-02	1.22	3.04	
6-4-090	4730	AF100	-47.1	53.5	0.18E+00	0.85	0.92	23.9
6-5-090	4880	AF100	49.8	289.4	0.48E-01	0.24	2.14	
6-6-090	5030	AF100	1.4	317.5	0.24E-01	0.22	5.42	
7-1-090	5240	AF100	28.9	126.0	0.94E-02	0.57	6.04	
7-2-090	5390	AF100	-33.0	49.2	0.25E-01	0.58	2.11	
7-3-090	5540	AF100	-14.7	113.4	0.30E-01	1.19	0.89	
7-4-090	5690	AF100	-75.8	60.0	0.17E-01	0.61	3.64	
7-5-090	5840	AF100	-23.8	132.6	0.12E-01	0.86	2.31	
7-6-090	5990	AF200	1.9	220.5	0.14E+00	0.46	1.17	19.0
8-1-090	6180	AF100	-71.8	52.2	0.14E-01	0.60	5.13	
8-2-090	6330	AF100	-29.0	90.5	0.78E+00	0.95	0.24	
8-3-090	6480	AF100	56.2	181.8	0.11E+00	0.93	0.58	
8-4-090	6630	AF050	11.5	336.5	0.44E-01	0.23	3.66	
8-5-090	6780	AF050	54.7	268.2	0.66E-01	0.79	1.00	
8-6-090	6930	AF050	-47.0	176.5	0.21E-01	0.82	2.11	
9-2-090	7300	AF300	-77.6	286.4	0.28E+00	0.75	0.64	64.0
9-3-090	7450	AF300	43.7	296.6	0.51E+00	0.50	1.04	30.0
9-4-089	7599	AF050	-71.6	126.4	0.29E-01	0.98	1.46	
9-4-091	7601	AF050	-49.6	22.7	0.62E-01	0.63	1.32	
9-5-090	7750	AF050	-46.4	2.2	0.20E-01	0.24	8.05	
9-6-088	7898	AF050	3.3	140.1	0.15E-01	0.54	2.80	
10-1-090	8060	AF050	-62.6	320.8	0.29E-01	0.81	2.13	
10-2-090	8210	NRM	*	*	0.66E-01	*	*	
10-3-090	8360	AF050	-29.4	97.1	0.70E-02	1.68	2.51	
10-4-090	8510	AF050	-11.3	228.3	0.73E-02	0.96	3.78	
10-5-090	8660	AF050	58.1	80.9	0.32E-01	0.81	1.18	
10-6-090	8810	AF200	-7.1	75.6	0.12E+00	0.34	1.81	13.5
11-1-115	9025	AF050	76.4	221.2	0.56E-01	1.18	0.51	
11-2-109	9169	AF050	25.4	5.8	0.68E-01	0.12	3.30	
11-3-109	9319	AF050	59.7	300.4	0.17E-01	1.11	0.96	
11-4-109	9469	AF050	58.2	302.7	0.26E-01	0.70	2.05	
11-5-109	9619	AF200	45.4	290.9	0.63E-01	0.39	2.93	8.9
11-6-116	9776	AF050	54.0	1.1	0.29E-01	0.70	2.24	

* Indicates no stable characteristic remanence found
NRM Jo Intensity of NRM in milliamps per meter
J/Jo Intensity of characteristic magnetization (at given step) divided by NRM intensity
CSD Circular standard deviation of characteristic remanence vector
MDF Mean destructive field, in milliTeslas

SAMPLE #	DEPTH (cm)	STEP	INCLI. (Down)	DECLI. (East)	NRM Jo (mA/m)	J/Jo	CSD	MDF (mT)
12-2-020	10020	AF050	76.2	248.6	0.39E-01	0.70	1.55	
12-3-020	10170	AF050	-10.7	83.0	0.23E-01	0.90	2.42	
12-4-136	10436	AF050	28.9	210.4	0.11E-01	1.03	3.02	
12-5-020	10470	AF050	56.3	270.6	0.10E-01	0.63	4.26	
12-5-091	10541	AF050	46.7	259.4	0.22E-01	0.74	1.48	
13-1-040	10830	AF050	73.7	14.9	0.53E-02	3.96	1.36	
13-2-040	10980	AF050	19.8	257.0	0.14E-01	0.80	3.34	
13-3-109	11199	AF050	-69.7	45.0	0.30E-01	1.11	1.01	
13-4-109	11349	AF050	-30.4	17.4	0.34E-01	0.94	1.10	
13-5-109	11499	AF050	-13.7	49.0	0.21E-01	0.52	3.68	
13-6-104	11644	AF050	42.3	183.0	0.14E-01	0.80	2.52	
13-7-019	11709	AF050	40.4	243.6	0.30E-01	0.47	2.93	
14-1-130	11870	AF100	21.2	285.0	0.50E-01	0.47	3.85	9.6
14-2-029	11919	AF050	13.9	54.4	0.32E-01	0.20	2.99	
14-2-130	12020	AF300	-66.7	297.4	0.14E+00	0.71	1.19	44.4
14-3-004	12044	AF050	-25.3	214.5	0.10E-01	0.59	4.94	
15-3-091	13091	TH200	-55.1	0.4	0.43E-01	0.25	4.18	
15-3-139	13139	AF050	68.7	245.3	0.55E-01	0.69	0.88	
16-1-060	13720	AF100	41.5	339.2	0.88E-02	0.65	7.99	
16-1-090	13750	AF050	81.9	223.3	0.71E-01	0.88	0.56	
16-1-140	13800	AF100	-27.9	324.1	0.14E-01	0.45	3.96	9.6
16-2-018	13828	AF100	27.6	295.5	0.20E-01	0.30	7.41	
16-2-041	13851	AF050	51.0	275.9	0.89E-02	1.34	1.63	
16-2-102	13912	AF100	60.1	335.5	0.13E-01	0.86	2.72	
16-3-031	13991	AF050	27.8	280.5	0.15E-01	0.77	1.61	
16-3-070	14030	AF100	26.2	354.4	0.20E-01	0.34	5.23	8.6
16-3-115	14075	AF100	72.7	150.6	0.14E-01	0.45	5.96	
16-4-020	14130	AF100	20.9	282.9	0.14E-01	0.57	4.85	
16-4-059	14169	AF050	-48.2	16.7	0.20E-01	0.41	4.53	
16-4-110	14220	AF150	61.8	53.9	0.70E-01	0.26	4.21	3.4
16-5-015	14275	AF200	19.2	320.3	0.98E+00	1.52	0.72	
16-5-059	14319	AF050	-52.2	351.1	0.24E-01	0.96	1.25	
16-5-135	14395	AF100	60.0	311.2	0.19E-01	0.35	7.20	
16-6-020	14430	AF100	45.6	25.8	0.12E-01	0.38	7.98	8.4
16-6-059	14469	AF300	-27.9	123.6	0.54E-01	0.24	2.60	24.6
16-6-120	14530	AF100	2.9	266.2	0.14E-01	0.51	6.02	8.5
17-1-020	14630	AF150	45.6	22.3	0.14E+00	0.28	2.35	4.4
17-1-050	14660	AF200	-50.3	6.6	0.15E+00	0.69	0.87	27.1
17-2-041	14801	AF050	-42.6	356.6	0.41E-01	0.81	0.84	
17-2-085	14845	AF100	8.5	204.0	0.96E-02	0.82	8.32	
17-2-130	14890	AF100	-49.6	44.2	0.28E-02	1.92	19.39	
17-3-041	14951	AF050	4.1	252.2	0.24E-01	1.00	1.53	
17-3-085	14995	AF100	29.8	17.3	0.19E-01	0.31	5.54	8.3
17-3-135	15045	AF150	47.9	290.8	0.18E-01	0.76	3.42	28.9
17-4-041	15101	AF050	40.1	340.7	0.28E-01	0.62	2.58	
17-4-085	15145	AF100	28.2	93.1	0.17E-01	0.81	4.54	
17-4-135	15195	AF100	32.3	169.6	0.19E-01	0.63	5.67	
17-5-041	15251	AF050	30.2	177.1	0.30E-01	0.38	2.29	3.9
17-5-090	15300	AF150	34.8	352.9	0.22E-01	0.48	4.37	9.4
17-6-041	15401	AF050	5.5	222.0	0.16E-01	0.89	1.28	
17-6-085	15445	AF200	73.3	66.5	0.42E-01	0.38	2.26	
17-6-130	15490	AF100	-5.5	62.8	0.49E-02	0.79	11.18	
18-1-030	15600	AF100	40.6	103.7	0.67E-02	0.63	8.82	9.2
18-1-070	15640	AF050	44.3	251.2	0.20E-01	0.97	1.94	
18-1-130	15700	AF100	-20.2	183.2	0.13E-01	0.37	13.05	

Abbreviations:

STEP Maximum step of demagnetization, (AF) alternating field or (TH) thermal, at which characteristic remanence direction was measured
INCLI. Inclination of characteristic remanence
DECLI. Declination of characteristic remanence

SAMPLE #	DEPTH (cm)	STEP	INCLI. (Down)	DECLI. (East)	NRM Jo (mA/m)	J/Jo	CSD	MDF (mT)
18-2-035	15755	AF100	39.5	136.7	0.17E-01	0.53	9.04	
18-2-070	15790	AF050	31.0	160.6	0.97E-02	1.08	4.27	
18-2-125	15845	AF100	32.2	42.9	0.14E-01	0.46	7.96	8.3
18-3-039	15909	AF200	36.6	297.7	0.77E-01	0.57	1.90	25.3
18-3-090	15960	AF050	-24.7	30.4	0.56E-02	1.15	17.59	
18-3-140	16010	AF100	42.8	190.7	0.35E-01	0.51	3.84	
18-4-039	16059	AF050	46.6	226.0	0.15E-01	0.38	4.39	
18-4-080	16100	AF050	-59.5	186.8	0.62E-02	0.55	7.24	
18-4-115	16135	AF150	58.0	303.7	0.24E-01	0.54	3.64	23.2
18-5-020	16190	AF050	-58.8	165.9	0.84E-02	0.68	10.70	
18-5-039	16209	AF050	31.4	166.4	0.30E-01	1.03	1.22	
18-5-080	16250	AF050	-61.4	159.1	0.80E-02	1.14	3.43	
18-6-039	16359	AF050	-21.3	147.9	0.15E-01	1.49	1.24	
18-6-111	16431	AF150	-60.7	58.2	0.12E+00	0.88	0.73	21.1
19-1-017	16537	AF200	-64.0	100.5	0.70E+00	0.56	0.78	21.6
19-1-070	16590	AF050	26.7	175.8	0.13E-01	0.36	14.48	
19-1-125	16645	AF050	69.0	153.1	0.18E-01	0.82	2.92	
19-2-017	16687	AF050	11.2	264.9	0.54E-01	0.65	6.18	6.9
19-2-090	16760	AF100	68.4	115.4	0.24E-01	0.29	7.36	6.3
19-2-130	16800	AF050	47.2	122.2	0.15E-01	0.34	5.38	
19-3-017	16837	AF050	10.9	175.8	0.36E-01	0.90	0.47	
19-3-070	16890	AF100	46.1	57.9	0.15E-01	0.50	8.16	
19-3-129	16949	AF050	-1.4	198.2	0.88E-02	0.41	9.37	
19-4-017	16987	AF050	32.6	45.0	0.26E-01	0.46	12.43	4.2
19-4-060	17030	AF100	-4.8	144.3	0.26E-01	0.40	5.98	8.3
21-1-040	18360	AF050	11.1	144.7	0.18E-01	0.79	5.78	
21-1-091	18411	AF050	17.9	15.9	0.27E-01	0.63	4.59	
21-1-140	18460	AF100	17.0	147.4	0.37E-01	0.09	12.78	
21-2-050	18520	AF300	8.0	7.4	0.44E-01	0.70	2.61	38.8
21-2-091	18561	AF050	62.3	43.0	0.21E-01	0.60	5.53	
21-3-035	18655	AF100	61.1	81.9	0.25E-01	0.53	4.85	
21-3-091	18711	AF050	17.7	299.8	0.26E-01	0.70	4.83	
21-3-130	18750	AF100	64.5	96.6	0.18E-01	0.52	7.36	
22-1-040	19310	AF200	-33.5	142.8	0.24E-01	0.65	4.51	
22-1-087	19357	AF050	48.7	58.3	0.47E-01	0.49	1.80	
22-1-130	19400	AF050	33.3	284.8	0.96E-02	0.94	2.76	
22-2-040	19460	AF050	24.7	161.9	0.11E-01	0.71	11.22	
22-2-090	19510	AF100	43.1	358.7	0.12E+00	0.67	1.07	13.7
22-2-130	19550	AF050	41.3	195.2	0.83E-02	0.54	22.35	
22-3-045	19615	AF100	28.1	281.3	0.11E-01	0.96	3.64	35.7
22-3-087	19657	AF050	52.1	355.7	0.14E-01	0.48	5.80	
22-3-135	19705	AF100	-49.7	274.2	0.36E-01	0.47	2.93	8.6
22-4-040	19760	AF100	58.6	138.7	0.24E-01	0.60	4.73	
22-4-087	19807	AF050	16.5	191.3	0.10E-01	2.23	0.81	
22-4-130	19850	AF050	-52.5	22.8	0.83E-02	0.95	3.36	
22-5-040	19910	AF050	50.4	13.1	0.13E-01	0.61	7.60	
22-5-087	19957	AF300	-68.9	179.9	0.13E+00	0.39	0.42	21.2
22-5-140	20010	AF050	4.7	15.3	0.76E-02	1.05	14.75	
22-6-040	20060	AF500	-4.8	304.0	0.25E-01	0.63	3.81	
22-6-090	20110	AF050	15.6	5.2	0.33E-01	0.42	3.97	3.9
22-6-130	20150	AF300	17.8	22.4	0.25E-01	0.63	8.58	34.5
23-1-037	20267	AF050	18.5	239.2	0.22E-01	0.39	5.22	
23-1-090	20320	AF050	46.4	132.5	0.13E-01	0.92	1.75	
23-1-140	20370	AF050	0.6	40.6	0.11E-01	0.85	7.81	
23-2-040	20420	AF200	-49.8	298.3	0.78E-02	1.20	3.06	

* Indicates no stable characteristic remanence found
NRM Jo Intensity of NRM in milliamps per meter
J/Jo Intensity of characteristic magnetization (at given step) divided by NRM intensity
CSD Circular standard deviation of characteristic remanence vector
MDF Mean destructive field, in milliTeslas

SAMPLE #	DEPTH (cm)	STEP	INCLI. (Down)	DECLI. (East)	NRM Jo (mA/m)	J/Jo	CSD	MDF (mT)
23-2-087	20467	AF050	0.9	258.8	0.64E-01	0.89	1.08	
23-2-130	20510	AF050	19.2	269.6	0.18E-01	0.59	3.94	
23-3-035	20565	AF100	-49.9	212.7	0.27E-01	0.58	3.23	
23-3-087	20617	AF050	-5.8	189.0	0.98E-02	0.19	15.07	2.9
23-3-130	20660	AF100	-49.5	89.5	0.67E-02	0.68	11.73	
23-4-040	20720	AF100	-11.4	321.7	0.20E-01	0.58	3.63	
23-4-090	20770	AF050	55.3	186.6	0.59E-01	0.86	0.67	
23-4-130	20810	AF050	-38.1	98.2	0.10E-01	1.90	2.26	
23-5-040	20870	AF100	9.5	2.8	0.20E-01	0.33	3.28	5.9
23-5-090	20920	AF050	27.3	20.5	0.29E-01	0.36	2.67	
23-5-140	20970	AF200	-48.5	246.5	0.48E-01	1.05	1.52	44.7
23-6-025	21005	AF050	-24.5	150.2	0.48E-01	1.17	1.02	
24-1-040	21230	AF100	-57.3	304.8	0.42E-01	1.02	2.38	
24-1-084	21274	AF050	60.1	80.2	0.61E-01	0.64	3.11	
24-1-130	21320	AF100	23.7	85.3	0.32E-01	0.36	5.00	7.5
24-2-035	21375	NRM	*	*	0.15E-01	*	*	
24-2-084	21424	AF050	20.3	102.1	0.12E-01	0.68	7.78	
24-2-140	21480	AF050	-14.6	25.6	0.11E-01	0.60	6.28	
25-1-045	22195	AF100	61.8	245.8	0.44E-01	0.84	2.41	
25-1-084	22234	AF050	29.0	8.4	0.87E-01	0.73	1.76	
25-2-030	22330	NRM	*	*	0.21E-01	*	*	
25-2-033	22333	AF050	27.7	29.1	0.54E-01	0.51	4.17	
25-2-100	22400	AF100	24.4	114.8	0.19E-01	0.83	4.62	
26-1-092	23232	AF050	40.1	33.5	0.21E+00	0.38	1.36	
26-1-137	23277	AF200	9.0	329.8	0.82E-01	0.82	1.77	
26-2-032	23322	AF050	14.1	358.7	0.11E+00	0.43	1.83	
26-2-070	23360	AF400	-56.7	353.2	0.61E-01	0.47	2.64	32.9
26-2-124	23414	AF300	8.0	0.5	0.29E+00	0.64	0.85	38.3
26-3-012	23452	AF300	-16.1	358.3	0.58E+00	0.31	0.77	4.8
26-3-069	23509	AF200	-4.4	3.6	0.96E+00	0.63	0.57	
27-1-047	24147	AF200	-52.2	100.5	0.57E-01	1.15	3.97	
27-1-129	24229	AF050	-32.2	350.0	0.47E-01	0.72	0.90	
27-2-040	24290	AF050	-27.3	261.5	0.56E-01	1.23	1.25	
27-2-091	24341	AF300	-36.3	25.3	0.36E-01	0.47	4.74	27.7
27-2-131	24381	AF100	-6.6	258.9	0.26E-01	0.95	1.89	
28-1-045	25105	AF050	24.3	8.5	0.11E-01	0.67	6.22	
28-1-074	25134	TH200	0.9	329.1	0.66E+00	0.89	0.30	
28-1-110	25170	AF050	37.6	39.6	0.44E-01	0.56	3.88	
28-2-030	25240	AF050	13.9	181.8	0.43E-01	1.20	1.69	
28-2-077	25287	AF300	16.3	45.5	0.47E-01	0.59	2.29	34.8
28-2-110	25320	AF050	5.3	207.0	0.11E-01	1.58	2.86	
28-3-018	25378	AF050	19.7	83.2	0.40E-01	0.73	3.68	
29-1-060	26080	AF050	-9.6	84.6	0.61E+01	0.03	0.47	
29-1-110	26130	AF050	13.7	122.9	0.10E+01	0.99	0.42	
29-2-012	26182	AF050	50.3	254.8	0.56E-01	0.42	3.15	
29-0-035	26312	AF050	-13.4	79.8	0.34E+00	0.30	0.85	
30-1-006	26996	AF050	-9.9	93.7	0.56E-01	0.64	3.14	
30-1-059	27049	AF050	-28.9	93.7	0.10E+00	0.91	0.26	
30-2-016	27156	AF050	27.5	131.4	0.16E+00	0.99	0.48	
30-2-113	27253	AF050	35.6	253.4	0.54E-01	0.91	0.93	
30-3-003	27293	TH300	47.5	294.5	0.19E+00	0.59	7.88	
30-3-027	27317	TH250	-33.1	146.3	0.92E+00	0.56	0.78	
30-0-003	27510	TH250	-64.1	357.1	0.29E+00	0.53	2.39	

Abbreviations:

STEP Maximum step of demagnetization, (AF) alternating field or (TH) thermal, at which characteristic remanence direction was measured
INCLI. Inclination of characteristic remanence
DECLI. Declination of characteristic remanence

SAMPLE #	DEPTH (cm)	STEP	INCLI. (Down)	DECLI. (East)	NRM Jo (mA/m)	J/Jo	CSD	MDF (mT)
13-1-049	11479	AF050	-6.7	91.1	0.13E-01	0.52	3.85	
13-2-049	11629	AF050	3.5	156.7	0.57E-02	2.53	2.94	
13-3-049	11779	AF800	-12.0	11.4	0.13E-01	0.48	29.62	
13-4-049	11929	AF700	-56.3	84.3	0.18E-01	0.22	18.90	14.8
13-5-049	12079	AF050	56.5	81.2	0.11E-01	0.85	4.93	
13-6-049	12229	AF050	38.2	224.7	0.21E-01	1.50	1.76	
13-7-028	12358	AF050	19.7	69.5	0.12E-01	0.54	6.65	
HOLE 631A								
1-1-030	30	AF200	15.4	66.3	0.12E-01	0.38	4.09	15.8
1-1-099	99	AF200	-23.0	291.8	0.11E+00	0.12	2.72	4.2
1-1-140	140	AF200	58.4	5.4	0.29E-01	0.35	3.56	12.8
1-2-029	179	AF050	-86.7	236.7	0.82E-01	0.94	0.53	
1-2-087	237	AF050	55.9	216.0	0.93E-02	1.23	4.29	
1-2-140	290	AF400	34.6	304.9	0.36E-01	0.14	6.30	26.1
1-3-015	315	AF050	58.3	307.9	0.43E-01	0.92	1.65	
1-3-075	375	AF300	61.5	72.6	0.30E-01	0.46	3.72	27.1
1-3-130	430	AF200	53.3	299.3	0.19E-01	0.54	4.20	21.5
1-4-030	480	AF050	-23.8	241.9	0.26E-01	0.86	1.43	
1-4-065	515	AF200	23.4	303.1	0.96E-02	0.57	18.21	24.5
1-4-099	549	AF050	26.4	321.2	0.25E-01	0.32	7.88	3.2
1-4-140	590	AF200	36.6	276.4	0.54E-01	0.32	3.36	13.1
1-5-030	630	AF200	42.4	252.5	0.37E+00	0.24	0.45	11.6
1-5-066	666	AF050	48.9	210.3	0.45E+00	0.26	0.40	3.4
1-5-115	715	AF200	40.8	259.1	0.51E+00	0.26	0.91	12.5
1-6-029	779	AF050	48.5	246.8	0.30E+00	0.40	0.57	3.9
1-6-080	830	AF200	41.1	251.3	0.14E+00	0.18	1.40	10.6
1-6-099	849	AF050	63.5	269.1	0.45E-01	0.67	1.09	
1-6-114	864	AF200	46.2	304.5	0.62E-01	0.29	1.89	11.9
1-7-026	926	AF050	21.9	92.3	0.96E-01	0.59	0.89	
2-1-020	990	AF200	39.4	19.6	0.71E-01	0.41	1.21	14.7
2-1-060	1030	AF300	43.7	18.0	0.11E+00	0.38	2.84	18.3
2-2-028	1148	AF100	-59.3	310.4	0.21E-01	0.53	4.09	33.1
2-2-080	1200	AF050	85.6	304.8	0.69E-01	0.74	1.29	
2-2-115	1235	AF200	49.6	232.4	0.21E+00	0.47	0.55	18.4
2-3-020	1290	AF200	-46.8	122.6	0.53E-01	0.45	1.39	17.1
2-3-088	1358	NRM	*	*	0.49E-01	*	*	
2-3-130	1400	AF200	-38.3	28.3	0.52E-01	0.31	6.70	6.8
2-4-020	1440	AF200	2.6	358.6	0.71E-01	0.31	1.79	13.8
2-4-088	1508	AF050	49.1	307.3	0.11E+00	0.74	0.54	
2-4-140	1560	AF200	18.8	20.8	0.90E-01	0.48	1.84	17.8
2-5-025	1595	AF200	51.8	207.9	0.12E+00	0.13	4.05	11.9
2-5-060	1630	AF050	37.6	277.8	0.81E-01	0.80	0.50	
2-5-115	1685	AF200	-34.7	41.0	0.40E-01	0.67	1.55	
2-6-020	1740	AF400	-40.1	108.2	0.19E-01	0.96	5.88	
2-6-060	1780	AF050	22.7	324.0	0.46E-01	0.37	1.50	3.7
2-6-120	1840	AF200	-26.6	53.8	0.45E-01	0.74	1.26	8.5
3-1-020	1980	AF200	-2.8	17.9	0.71E-01	0.43	1.48	18.0
3-1-069	2029	AF100	7.8	5.3	0.18E+00	0.23	2.22	6.5
3-1-114	2074	AF050	-35.0	160.6	0.24E-01	1.33	2.29	
3-2-020	2130	AF400	-49.7	228.5	0.18E-01	0.75	4.50	
3-2-070	2180	AF050	-28.4	103.1	0.37E-02	1.71	11.19	
3-2-114	2224	AF300	-4.0	34.9	0.99E-01	0.44	14.30	27.3
3-3-018	2278	AF300	73.8	182.4	0.25E-01	0.60	6.72	
3-3-070	2330	AF100	41.7	244.2	0.15E-01	0.75	3.99	

* Indicates no stable characteristic remanence found
NRM Jo Intensity of NRM in milliamps per meter
J/Jo Intensity of characteristic magnetization (at given step) divided by NRM intensity
CSD Circular standard deviation of characteristic remanence vector
MDF Mean destructive field, in milliTeslas

SAMPLE #	DEPTH (cm)	STEP	INCLI. (Down)	DECLI. (East)	NRM Jo (mA/m)	J/Jo	CSD	MDF (mT)
3-3-120	2380	AF050	27.8	283.9	0.29E-02	1.47	4.81	
3-4-020	2430	AF050	3.3	145.3	0.28E-02	2.11	11.29	
3-4-065	2475	AF300	-5.5	72.0	0.12E-01	0.19	12.91	4.0
3-4-114	2524	AF050	-81.6	117.7	0.38E-01	0.97	2.41	
3-5-020	2580	AF300	-41.9	352.6	0.11E-01	0.41	44.87	
3-5-061	2621	AF300	59.1	95.6	0.13E-01	0.82	23.55	34.0
3-5-114	2674	AF050	-51.3	272.9	0.43E-01	0.79	1.93	
3-6-033	2743	AF200	51.2	55.3	0.29E-02	2.21	10.44	
3-6-079	2789	AF050	-25.7	8.7	0.61E-02	0.57	21.69	
3-6-114	2824	AF050	-34.5	291.4	0.25E-01	1.92	1.73	
4-1-061	3011	AF100	68.3	53.3	0.14E-01	0.25	8.52	3.6
4-1-117	3067	AF200	-64.9	55.2	0.56E-01	0.36	3.47	
4-2-050	3150	AF050	59.8	22.9	0.87E-02	0.49	21.69	
4-2-100	3200	AF050	15.2	288.7	0.96E-03	6.12	9.51	
4-3-048	3298	AF050	44.8	329.9	0.98E-02	0.33	12.71	
4-3-101	3351	AF100	48.4	60.3	0.12E-01	0.57	10.10	9.5
4-4-048	3448	AF050	-31.2	203.2	0.16E-02	2.16	23.12	
4-4-137	3537	AF050	20.4	275.3	0.35E-01	0.33	4.65	
4-6-060	3760	AF100	24.1	21.8	0.12E-01	0.76	7.70	
4-6-115	3815	AF050	19.4	141.5	0.13E-01	1.07	3.42	
6-1-050	4920	AF300	56.6	46.6	0.83E-01	0.35	5.50	18.5
6-2-050	5070	AF050	-44.8	315.0	0.14E-01	0.71	15.90	
6-3-090	5260	AF050	-12.3	93.4	0.38E-01	0.50	2.08	
6-4-050	5370	AF200	-23.0	357.9	0.48E-01	0.22	15.40	4.4
6-5-050	5520	AF050	32.3	351.3	0.31E-01	0.85	0.89	
6-6-050	5670	AF050	53.6	334.9	0.29E-01	0.83	0.57	
7-2-035	6005	AF050	63.6	353.8	0.34E-01	0.87	1.84	
7-3-018	6138	AF050	77.5	276.7	0.30E-01	0.85	1.72	
7-4-060	6330	AF050	-67.7	203.2	0.21E-01	0.84	2.94	
7-5-060	6480	AF050	48.0	295.0	0.56E-01	0.59	1.13	
7-6-119	6689	AF050	76.0	348.3	0.34E-01	0.67	1.75	
7-7-017	6737	AF050	-84.4	284.8	0.18E-01	0.40	4.90	
8-1-088	6888	AF300	36.5	313.3	0.10E+00	0.57	2.33	
8-2-020	6970	AF050	-2.2	32.4	0.41E-01	0.48	1.79	
8-3-094	7194	AF050	-40.7	207.2	0.51E-01	1.46	0.47	
8-4-020	7270	AF050	-2.1	255.0	0.25E-01	1.16	1.52	
8-5-020	7420	AF050	34.7	222.6	0.13E-01	1.33	3.01	
8-6-020	7570	AF050	15.2	44.0	0.80E-01	0.81	0.61	
8-7-016	7716	AF050	63.0	27.7	0.39E-01	0.59	1.13	
HOLE 632A								
1-1-011	11	AF500	58.9	233.8	0.29E+01	0.47	0.40	46.3
1-1-040	40	TH350	80.9	298.9	0.22E+01	0.56	0.41	
1-1-110	110	AF300	87.3	35.7	0.23E+01	0.55	0.60	37.1
1-1-141	141	AF500	72.1	223.2	0.51E+01	0.39	1.00	
1-2-011	161	AF500	62.0	247.9	0.57E+01	0.49	0.56	
1-2-040	190	AF400	56.1	253.1	0.97E+01	0.42	0.52	31.1
1-2-081	231	AF500	54.9	248.3	0.73E+01	0.25	0.28	
1-2-110	260	AF100	77.5	188.3	0.48E+01	0.34	0.41	7.6
1-3-011	311	AF500	72.9	188.9	0.43E+01	0.24	0.38	
1-3-040	340	AF100	69.1	62.5	0.22E+01	0.37	0.48	7.8
1-3-080	380	AF500	76.8	137.5	0.28E+01	0.18	0.17	
1-3-110	410	AF100	53.9	140.4	0.28E+01	0.39	0.34	8.2
1-4-011	461	AF500	63.1	109.3	0.29E+01	0.31	0.46	
1-4-040	490	AF300	67.3	104.1	0.45E+01	0.35	0.66	16.4

Abbreviations:

STEP Maximum step of demagnetization, (AF) alternating field or (TH) thermal, at which characteristic remanence direction was measured
INCLI. Inclination of characteristic remanence
DECLI. Declination of characteristic remanence

SAMPLE #	DEPTH (cm)	STEP	INCLI. (Down)	DECLI. (East)	NRM Jo (mA/m)	J/Jo	CSD	MDF (mT)
1-4-085	535	AF500	52.2	184.6	0.33E+01	0.15	0.45	
1-4-110	560	AF100	66.3	183.5	0.27E+01	0.41	0.48	8.5
1-5-020	620	AF100	44.5	218.8	0.48E+01	0.37	0.17	7.8
2-1-020	710	AF600	23.9	16.0	0.35E+00	0.13	1.79	25.3
2-1-071	761	AF500	31.7	331.8	0.14E+01	0.22	0.79	
2-1-124	814	AF100	7.3	41.7	0.22E+01	0.34	0.55	7.6
2-2-020	860	TH300	31.2	357.4	0.25E+00	0.66	0.76	
2-2-066	906	AF600	15.3	346.2	0.26E+00	0.26	2.60	
2-2-099	939	AF300	52.1	286.3	0.19E+00	0.47	2.59	27.3
2-2-129	969	AF500	40.3	335.8	0.24E+00	0.26	1.69	
2-3-019	1009	AF500	56.5	121.8	0.19E+00	0.26	1.28	
2-3-093	1083	AF100	28.4	148.7	0.24E+00	0.72	1.03	14.6
2-3-129	1119	AF500	28.1	71.8	0.49E-01	0.55	5.06	
2-4-017	1157	AF100	13.9	120.1	0.92E-01	0.81	1.59	23.1
2-4-060	1200	AF500	36.8	354.6	0.14E+00	0.20	1.90	
2-4-099	1239	AF200	47.4	342.8	0.36E+00	0.11	11.08	5.2
2-4-139	1279	AF500	31.5	29.6	0.79E-01	0.51	1.93	
2-5-016	1306	AF100	59.2	148.6	0.80E-01	0.68	2.41	24.8
2-5-070	1360	AF500	31.1	70.7	0.74E-01	0.48	2.22	
2-5-100	1390	AF100	52.4	95.5	0.46E-01	0.74	7.03	22.0
2-5-130	1420	AF500	40.0	97.7	0.51E-01	0.57	2.71	
2-6-020	1460	AF400	42.4	101.0	0.58E-01	0.46	1.52	32.0
2-6-069	1509	AF500	20.2	60.1	0.39E-01	0.20	7.59	
2-6-099	1539	AF300	45.4	102.1	0.22E+00	0.09	4.69	2.9
3-1-018	1688	AF500	72.2	119.7	0.56E-01	1.06	1.74	79.5
3-3-049	2019	AF100	54.4	89.4	0.67E-01	0.38	5.66	7.7
3-3-093	2063	AF500	27.5	25.8	0.38E-01	0.23	8.06	
3-3-120	2090	AF100	-64.8	24.5	0.67E-01	0.69	2.54	15.7
3-4-011	2131	AF100	25.6	10.1	0.40E-01	0.71	2.31	19.6
3-4-049	2169	AF200	47.1	50.5	0.12E+00	0.40	3.23	12.8
3-4-112	2232	AF300	28.0	298.9	0.15E+00	0.67	4.07	56.7
3-5-040	2310	AF200	42.7	339.3	0.99E-01	0.52	0.62	21.1
3-5-070	2340	AF600	18.1	325.1	0.18E+00	0.47	1.29	55.0
3-5-101	2371	AF100	40.3	51.0	0.48E-01	0.23	9.84	6.3
3-6-023	2443	AF100	17.5	359.0	0.83E-02	1.29	4.22	
3-6-089	2509	AF100	47.7	29.7	0.26E-01	0.46	1.85	8.3
4-1-045	2675	AF700	73.1	96.8	0.10E+03	0.39	1.09	35.0
4-1-130	2760	AF600	-59.1	354.5	0.53E+00	0.48	1.81	56.0
4-2-040	2820	AF100	32.6	32.4	0.12E-01	0.92	2.76	
4-2-110	2890	AF600	48.6	24.3	0.47E-01	0.49	4.32	59.0
4-3-040	2970	AF100	-38.6	110.2	0.86E-02	0.56	7.48	
4-3-130	3060	AF100	1.8	66.9	0.10E-01	0.48	7.93	8.9
4-4-041	3121	AF100	-13.4	357.7	0.14E-01	1.08	14.28	
4-4-111	3191	AF100	-27.8	121.6	0.11E-01	0.45	6.49	8.3
4-5-041	3271	AF200	-42.4	306.3	0.15E+00	0.11	6.36	
9-1-080	7500	NRM	*	*	0.50E-01	*	*	
10-1-090	8470	AF300	58.0	156.3	0.21E-01	0.28	7.00	22.0
12-1-073	9463	AF400	-66.8	200.3	0.58E-01	0.68	1.29	49.1
12-2-055	9595	AF200	-12.4	132.2	0.37E-01	0.19	8.08	
12-3-081	9771	AF500	73.2	125.4	0.22E-01	1.02	1.72	
12-4-081	9921	AF200	-38.8	89.2	0.38E-01	0.28	4.28	15.3
12-5-078	10068	AF200	-7.6	103.4	0.35E-01	0.29	3.90	14.9
12-6-081	10221	AF200	-12.8	188.9	0.63E-01	0.67	2.63	24.4

* Indicates no stable characteristic remanence found
NRM Jo Intensity of NRM in milliamps per meter
J/Jo Intensity of characteristic magnetization (at given step) divided by NRM intensity
CSD Circular standard deviation of characteristic remanence vector
MDF Mean destructive field, in milliTeslas

SAMPLE #	DEPTH (cm)	STEP	INCLI. (Down)	DECLI. (East)	NRM Jo (mA/m)	J/Jo	CSD	MDF (mT)
4-1-009	14969	TH200	14.1	144.9	0.86E-01	0.79	0.89	
4-1-110	15070	AF300	38.2	56.2	0.21E+00	0.15	1.32	12.7
6-1-053	16943	TH200	-27.0	105.9	0.40E-01	0.62	1.37	
6-1-093	16983	TH200	-31.7	214.3	0.47E-01	0.53	2.35	
7-1-089	17949	TH200	-34.8	30.1	0.00E+00	0.00	0.27	
7-1-112	17972	TH700	-34.6	221.7	0.24E+00	0.06	14.35	
9-1-055	19845	TH200	-19.7	269.1	0.28E-01	0.54	2.08	
9-1-070	19860	TH300	23.0	210.0	0.12E-01	0.36	15.19	
12-1-055	22725	TH200	10.1	353.4	0.18E-01	0.97	3.77	
12-1-142	22812	TH300	62.7	335.9	0.40E-01	0.21	2.47	
12-2-026	22846	TH200	50.2	192.2	0.11E+00	0.71	0.34	
13-1-004	23634	TH200	81.2	107.8	0.00E+00	0.00	1.16	
13-0-006	23750	TH200	-28.2	350.9	0.00E+00	0.00	0.38	
15-3-126	25976	TH400	-39.0	85.0	0.66E-01	0.23	1.72	
16-0-009	26886	AF400	42.5	33.8	0.42E-01	0.16	3.54	
HOLE 633A								
1-1-021	21	AF500	45.2	53.8	0.50E+01	0.43	0.70	43.0
1-1-071	71	AF400	37.6	22.4	0.53E+01	0.42	0.63	32.7
1-1-114	114	TH350	35.5	36.6	0.22E+01	1.50	0.23	
1-2-030	180	AF500	39.4	48.5	0.82E+01	0.39	0.63	40.0
1-2-081	231	AF400	31.4	3.8	0.36E+01	0.24	0.58	20.7
1-2-114	264	AF400	47.0	12.4	0.18E+01	0.41	0.76	33.1
1-3-041	341	AF400	26.5	37.5	0.46E+01	0.31	0.52	24.3
1-3-091	391	AF400	28.7	26.2	0.56E+01	0.31	0.38	27.5
1-3-114	414	AF300	30.5	42.8	0.27E+01	0.38	0.85	19.6
1-4-041	491	AF400	32.3	20.6	0.50E+01	0.45	0.51	35.8
1-4-081	531	AF400	32.9	16.0	0.77E+01	0.40	0.54	32.9
1-4-114	564	AF300	37.3	21.9	0.59E+01	0.32	0.72	19.2
1-5-021	621	AF400	34.0	57.2	0.59E+01	0.30	0.44	24.7
1-5-035	635	AF100	26.6	29.7	0.93E+00	0.03	1.65	5.2
1-5-071	671	AF400	29.9	31.8	0.10E+01	0.24	1.04	23.3
1-5-114	714	AF300	34.8	58.5	0.29E+01	0.29	0.80	16.7
1-6-058	808	AF300	-0.1	52.8	0.56E+01	0.25	1.00	15.9
2-1-021	891	AF400	66.1	105.0	0.27E+01	0.46	2.05	36.0
2-1-055	925	AF300	63.9	170.1	0.95E+00	0.38	0.27	20.8
2-1-111	981	AF400	50.0	42.7	0.15E+01	0.23	0.36	19.3
2-2-021	1041	AF400	31.6	11.5	0.14E+01	0.24	0.46	20.0
2-2-055	1075	AF300	39.4	9.5	0.76E+00	0.33	0.90	23.8
2-2-111	1131	AF200	50.4	302.3	0.34E+00	0.16	27.58	6.6
2-3-020	1190	AF300	38.3	71.4	0.41E+00	0.45	0.57	25.7
2-3-055	1225	AF200	50.5	63.0	0.93E+00	0.12	5.75	7.1
2-3-111	1281	AF300	32.5	65.5	0.79E-01	0.47	1.98	26.3
2-4-021	1341	AF500	39.4	80.8	0.41E-01	0.41	10.22	45.3
2-4-055	1375	AF300	39.1	148.7	0.49E-01	0.61	0.95	36.7
2-4-110	1430	AF400	33.3	82.1	0.10E+00	0.28	2.31	25.0
2-5-020	1490	AF300	41.8	88.5	0.12E+00	0.45	1.31	25.4
2-5-055	1525	AF600	26.1	74.0	0.31E+00	0.26	1.07	26.0
2-5-110	1580	AF400	21.0	90.5	0.94E-01	0.43	2.73	23.6
2-6-021	1641	AF300	38.3	31.7	0.16E+00	0.43	0.50	23.8
2-6-055	1675	AF300	42.7	40.1	0.62E-01	0.41	1.82	26.3
2-6-091	1711	AF300	39.4	338.7	0.11E+00	0.28	1.26	14.5
3-1-011	1841	AF900	-40.3	37.3	0.49E+00	0.46	5.40	
3-1-050	1880	AF300	-54.5	28.0	0.32E-01	0.17	16.41	15.9
3-1-111	1941	AF500	-28.1	30.2	0.23E-01	0.66	4.10	

Abbreviations:

STEP Maximum step of demagnetization, (AF) alternating field or (TH) thermal, at which characteristic remanence direction was measured
INCLI. Inclination of characteristic remanence
DECLI. Declination of characteristic remanence

SAMPLE #	DEPTH (cm)	STEP	INCLI. (Down)	DECLI. (East)	NRM Jo (mA/m)	J/Jo	CSD	MDF (mT)
3-2-010	1990	AF100	25.3	10.7	0.10E-01	0.70	4.19	
3-2-050	2030	TH200	-4.5	35.5	0.24E-01	0.59	2.76	
3-2-111	2091	AF200	-45.5	351.6	0.28E-01	0.65	4.25	
3-3-009	2139	AF500	-47.5	353.1	0.45E-01	0.51	2.17	50.0
3-3-050	2180	AF300	-35.2	256.9	0.54E-01	0.49	3.18	29.0
3-3-110	2240	AF200	-40.2	347.9	0.30E-01	0.64	1.86	
3-4-010	2290	NRM	*	*	0.38E-01	*	*	
3-4-110	2390	AF300	-23.7	86.5	0.79E-01	0.75	2.35	39.6
3-5-023	2453	AF400	-44.3	348.3	0.38E-01	1.05	1.42	
3-5-050	2480	AF500	-52.1	320.3	0.18E-01	1.02	4.34	
3-5-111	2541	AF300	-33.0	333.8	0.20E-01	0.96	2.48	
3-6-011	2591	AF200	-37.8	334.8	0.91E-01	0.29	2.87	7.8
3-6-050	2630	AF300	-29.7	351.8	0.41E-01	0.75	3.33	58.4
3-6-111	2691	AF200	-38.8	297.1	0.46E-01	0.81	2.44	33.7
4-1-021	2821	AF400	-37.7	194.6	0.79E-02	2.25	2.60	
4-1-070	2870	AF300	-38.7	25.1	0.57E-01	0.50	0.95	29.5
4-2-021	2971	AF300	-40.1	178.5	0.67E-01	0.51	2.11	29.2
4-2-119	3069	AF400	-35.9	103.7	0.59E-01	0.54	1.03	44.0
4-3-011	3111	AF300	-56.9	124.3	0.95E-02	0.73	4.07	28.3
4-3-101	3201	AF400	-39.3	143.2	0.34E-01	0.70	2.29	
4-4-020	3270	AF500	-37.8	122.3	0.39E-01	0.46	3.47	46.0
4-4-061	3311	AF500	-39.8	120.4	0.67E-01	0.54	1.46	
4-4-120	3370	AF500	-43.0	202.3	0.23E-01	0.86	2.70	66.2
4-5-041	3441	AF500	-47.8	221.8	0.26E-01	0.53	2.52	
4-5-110	3510	AF400	-46.0	137.6	0.24E-01	0.93	1.38	
4-6-020	3570	AF200	-31.9	150.8	0.36E-01	1.35	0.99	
4-6-115	3665	AF300	-18.6	98.4	0.36E-01	0.55	2.21	35.0
5-1-052	3812	AF200	-27.4	354.1	0.22E+01	0.65	0.21	
5-1-120	3880	AF100	-25.7	42.3	0.15E-01	1.19	3.32	
5-2-040	3950	AF100	21.0	265.2	0.47E-01	0.32	2.92	7.6
5-2-100	4010	AF200	27.7	203.0	0.75E-01	0.41	1.76	16.4
5-3-042	4102	AF200	84.4	223.7	0.11E+00	0.44	0.83	17.5
5-3-120	4180	AF200	37.7	223.7	0.72E-01	0.40	1.71	17.6
5-4-040	4250	AF200	-42.7	105.8	0.27E+00	1.02	0.18	
5-4-120	4330	AF100	13.1	49.1	0.28E-01	0.34	8.16	8.3
5-5-039	4399	AF300	-24.6	356.1	0.24E-01	0.77	4.17	38.0
5-5-110	4470	AF500	-35.2	38.6	0.31E-01	0.67	5.91	64.3
5-6-050	4560	AF100	-0.7	74.9	0.87E-02	1.12	6.16	
5-6-120	4630	AF200	-33.6	286.2	0.44E-01	0.25	3.24	13.2
6-1-050	4770	AF300	65.1	37.5	0.16E-01	1.03	9.80	
6-1-120	4840	AF200	46.3	102.8	0.11E+00	0.25	1.77	
6-2-050	4920	AF100	-34.0	68.1	0.71E-02	1.15	4.54	
6-2-110	4980	AF300	20.2	328.8	0.40E-02	2.66	3.91	80.2
6-3-040	5060	AF100	33.5	39.8	0.55E-02	0.76	9.73	9.8
6-3-110	5130	AF100	-84.2	33.2	0.21E-01	0.99	2.10	
6-4-040	5210	AF050	30.0	35.3	0.24E-01	0.24	7.61	3.1
6-4-091	5261	AF200	-7.2	229.5	0.38E-01	0.41	3.17	17.9
6-5-061	5381	AF100	-14.2	39.4	0.81E-02	0.82	12.81	
6-6-055	5525	AF100	-19.6	199.2	0.12E-01	0.92	5.77	
6-6-130	5600	AF400	40.3	300.7	0.15E-01	0.92	4.85	
7-1-121	5811	AF100	15.5	83.1	0.20E-01	0.74	5.94	
7-2-045	5885	AF200	-31.0	101.9	0.61E-01	0.40	2.10	
7-2-120	5960	AF200	-24.6	62.6	0.15E-01	0.48	5.00	12.9
7-3-040	6030	AF100	-74.0	281.1	0.74E-02	0.93	3.33	
7-3-110	6100	AF100	39.9	283.2	0.45E-01	0.86	1.26	

* Indicates no stable characteristic remanence found
NRM Jo Intensity of NRM in milliamps per meter
J/Jo Intensity of characteristic magnetization (at given step) divided by NRM intensity
CSD Circular standard deviation of characteristic remanence vector
MDF Mean destructive field, in milliTeslas

SAMPLE #	DEPTH (cm)	STEP	INCLI. (Down)	DECLI. (East)	NRM Jo (mA/m)	J/Jo	CSD	MDF (mT)
7-4-040	6180	AF100	40.9	6.7	0.12E-01	0.98	2.41	
7-4-110	6250	AF300	20.3	274.1	0.46E+00	0.37	1.23	24.1
7-5-040	6330	AF100	17.6	74.0	0.11E-01	0.80	4.52	
7-5-110	6400	AF100	-15.9	48.6	0.18E-01	0.67	4.18	
7-6-060	6500	AF300	22.4	101.1	0.38E-01	0.56	2.49	32.0
8-2-049	6839	AF100	17.0	160.5	0.24E-01	1.05	1.86	
8-3-040	6980	AF200	65.2	204.2	0.50E+00	0.32	0.59	14.7
8-3-095	7035	AF200	20.1	359.2	0.51E-01	0.34	2.30	12.9
8-4-025	7115	AF100	60.3	268.8	0.31E-01	0.54	2.80	9.8
8-4-090	7180	AF300	24.1	288.5	0.11E+00	0.13	2.07	14.8
HOLE 634A								
2-1-053	14453	TH300	63.3	52.7	0.15E+00	0.70	0.45	
2-1-121	14521	AF800	6.0	68.0	0.43E+01	0.33	1.02	
2-2-046	14596	TH300	37.2	17.1	0.17E+00	0.66	0.31	
2-2-112	14662	TH300	-2.1	202.5	0.16E+00	0.77	0.58	
2-3-033	14733	TH400	-28.7	338.8	0.60E-01	0.88	1.78	
2-3-086	14786	TH300	-28.5	279.9	0.75E-01	1.33	0.67	
2-3-142	14842	NRM	*	*	0.49E+00	*	*	
2-4-046	14896	TH300	36.9	16.3	0.29E+00	0.37	0.85	
2-4-110	14960	TH400	-31.9	48.7	0.11E+01	0.24	3.04	
2-5-018	15018	TH300	62.5	300.2	0.16E+01	0.19	0.24	
2-5-093	15093	TH450	-29.3	48.2	0.17E+01	0.14	5.06	
4-1-024	16334	TH300	-31.7	276.4	0.19E+00	0.77	0.16	
4-1-080	16390	TH300	47.5	136.4	0.12E+00	0.20	0.83	
4-1-129	16439	AF500	-35.9	264.7	0.17E+00	0.40	0.77	43.8
4-2-053	16513	TH300	23.1	326.4	0.82E-01	0.30	0.91	
4-2-110	16570	TH300	-25.9	7.6	0.12E+00	0.79	0.32	
4-3-023	16633	TH300	-23.0	101.3	0.92E-01	1.11	0.34	
4-3-052	16662	TH500	-28.6	61.3	0.23E+00	0.16	1.31	
HOLE 635B								
3-1-032	1362	TH200	30.1	21.1	0.60E-01	0.59	1.32	
3-1-079	1409	TH200	59.1	40.4	0.64E-01	0.38	2.79	
8-1-024	6124	TH200	39.5	305.3	0.14E-01	0.58	9.84	
8-1-061	6161	TH250	-45.5	206.0	0.15E-01	0.69	6.75	
8-2-040	6290	AF200	47.6	26.3	0.98E-01	0.07	3.06	4.0
10-1-027	8047	TH250	47.2	332.2	0.47E-01	0.24	1.82	
10-1-127	8147	TH350	57.0	48.1	0.70E-01	0.09	5.87	
10-2-032	8202	TH300	47.2	71.1	0.41E-01	0.26	7.04	
10-2-098	8268	TH250	41.8	327.2	0.41E-01	0.27	3.94	
10-3-040	8360	TH200	32.5	100.8	0.25E-01	0.36	6.07	
11-1-017	8977	AF200	78.3	153.7	0.54E-01	0.17	3.71	
11-1-133	9093	TH200	17.9	204.5	0.22E-01	0.57	5.81	
11-2-016	9126	TH250	35.0	236.3	0.29E-01	0.22	6.80	
11-2-114	9224	TH250	-60.5	91.6	0.13E-01	0.32	10.95	
12-1-014	9924	TH250	52.7	247.8	0.37E-01	0.17	10.64	
12-1-084	9994	TH250	43.5	302.5	0.40E-01	0.25	3.80	
12-2-005	10065	TH200	34.0	340.1	0.29E-01	0.33	3.95	
12-2-103	10163	TH200	83.3	100.4	0.77E-01	0.19	8.02	
13-1-028	10858	TH200	30.2	253.0	0.43E-01	0.53	9.76	
13-1-123	10953	TH150	63.6	255.0	0.28E-01	0.29	4.11	
13-1-137	10967	NRM	*	*	0.26E-01	*	*	
13-2-091	11071	TH200	36.4	32.5	0.25E-01	0.27	9.35	
13-2-131	11111	TH300	45.7	36.5	0.12E+00	0.35	3.58	